

Mitigating the efflorescence of alkali-activated slag mortars by aluminosilicate-based lightweight fine aggregate

Liu, Chen; Li, Zhenming; Ye, Guang

DOI

10.1016/j.cemconres.2025.107917

Publication date

Document Version Final published version

Published in

Cement and Concrete Research

Citation (APA)

Liu, C., Li, Z., & Ye, G. (2025). Mitigating the efflorescence of alkali-activated slag mortars by aluminosilicate-based lightweight fine aggregate. *Cement and Concrete Research*, *195*, Article 107917. https://doi.org/10.1016/j.cemconres.2025.107917

Important note

To cite this publication, please use the final published version (if applicable). Please check the document version above.

Copyright

Other than for strictly personal use, it is not permitted to download, forward or distribute the text or part of it, without the consent of the author(s) and/or copyright holder(s), unless the work is under an open content license such as Creative Commons.

Please contact us and provide details if you believe this document breaches copyrights. We will remove access to the work immediately and investigate your claim.

ELSEVIER

Contents lists available at ScienceDirect

Cement and Concrete Research

journal homepage: www.elsevier.com/locate/cemconres



Mitigating the efflorescence of alkali-activated slag mortars by aluminosilicate-based lightweight fine aggregate

Chen Liu^a, Zhenming Li^{b,c,*}, Guang Ye^{a,**}

- a Department of Materials and Environment (Microlab), Faculty of Civil Engineering and Geoscience, Delft University of Technology, 2628, CN, Delft, the Netherlands
- ^b School of Civil and Environmental Engineering, Harbin Institute of Technology, 518000 Shenzhen, China
- ^c Guangdong Provincial Key Laboratory of Intelligent and Resilient Structures for Civil Engineering, Harbin Institute of Technology, 518000 Shenzhen, China

ARTICLE INFO

Keywords: Efflorescence Alkali-activated slag Lightweight fine aggregate Leaching Pozzolanic reaction

ABSTRACT

Efflorescence is a significant aesthetic and structural issue for alkali-activated materials (AAMs). This study addressed this issue at the aggregate level for the first time. The results indicated that substituting sand with aluminosilicate-based lightweight fine aggregate (LWFA) by 20 % or 50 % in volume reduced the efflorescence of alkali-activated slag (AAS) mortars by 14.6 % or 43 %, respectively. The mitigation mechanisms of LWFA were proposed in terms of gels, pore solution and microstructure. Specifically, the pozzolanic reaction of LWFA provided gels with additional Si and Al, which contributed to binding Na⁺ in the pore solution, thereby reducing the available Na for efflorescence formation. Combined with its internal curing effect, LWFA densified the surrounding pastes, which hindered the transport of ions and water, thus limiting the formation of efflorescence products. Furthermore, the incorporation of LWFA enhanced the flexural strength of mortars without significantly compromising compressive strength.

1. Introduction

Efflorescence refers to the occurrence of whitish deposits that occasionally manifest on or in proximity to the surface of porous construction and building materials [1]. The formation of efflorescence products contains a succession of physiochemical reactions, primarily characterized by the interaction between dissolved alkali (earth) metal ions with carbonate ions. As a consequence of the limited availability of alkali metal ions, efflorescence products predominantly consist of calcium carbonate in cementitious materials [2]. These products typically exhibit a loose and fluffy texture [3], which is merely considered an aesthetic problem [4].

However, efflorescence in alkali-activated materials (AAMs) is much more pronounced than in OPC materials, attributed to the unique chemistry involved. The activation process of precursors introduces a large amount of alkali metal ions. Na, as the most prevalently used alkali metal ion, usually shows weaker bonding within the gel structure and higher mobility in the pore solution than Ca [5]. These characteristics facilitate the migration of Na to the surface of materials under moist conditions, where Na can react with (bi)carbonate ions to the formation of sodium (bi)carbonate [6–10]. The excessive formation of

efflorescence products has the potential to induce considerable expansion, which can be detrimental to the stability of the matrix [11,12]. Hence, efflorescence in AAMs is not only a cosmetic concern but could potentially evolve into a structural issue.

Many scholars have dedicated their efforts to elucidating the influential factors governing the efflorescence of AAMs. It is found that a higher dosage of alkali contributes to a denser microstructure and higher strength, while more significant efflorescence formation [13,14]. Efflorescence also depends on the type of alkali metal ions present in activators. Maghsoodloorad et al. [15] observed that the inclusion of potassium hydroxide can effectively suppress the visible efflorescence of alkali-activated phosphorus slag. A similar finding was reported based on geopolymer materials as well [16]. Both studies attributed the reduction of efflorescence to the high solubility of potassium carbonate. In addition to the pore solution, gel chemistry also plays a significant role in the efflorescence formation of AAMs. Yao et al. [17,18] investigated the impact of slag content (0 %, 25 %, 50 %, 75 % and 100 %) on the efflorescence of alkali-activated slag and fly ash (AASF) pastes. Their findings revealed that a low substitution of slag (<50 %) exhibited limited influence on efflorescence. Instead, high slag content (higher than 50 %) exhibited a rapid efflorescence than those without slag

E-mail addresses: C.Liu-12@tudelft.nl (C. Liu), zhenmingli@hit.edu.cn (Z. Li), G.Ye@tudelft.nl (G. Ye).

^{*} Correspondence to: Z. Li, School of Civil and Environmental Engineering, Harbin Institute of Technology, 518000 Shenzhen, China.

^{**} Corresponding author.

incorporation. They attributed this to the distinction between C-(N-)A-S-H gels and N-(A-)S-H gels, as the binding of Na in N-(A-)S-H gels is more robust than that in C-(N-)A-S-H gels [19]. However, different findings were reported by Srinivasamurthy et al. [20], who found that the inclusion of slag (ranging from 10 % to 30 %) benefits in reducing the efflorescence of AASF pastes. Slag normally has a higher reactivity than fly ash, which contributes to the formation of gels and the reduction of porosity. Zhang et al. [7,11] discovered that the incorporation of soluble Si-based activators can effectively reduce the initial efflorescence of geopolymer. These results indicate that a dense microstructure can impede the ion transport within the matrix, consequently lowering the visible efflorescence of AAMs [8,14,20–23]. Therefore, the density of the microstructure serves as another influential factor governing efflorescence.

Various mitigation strategies for efflorescence have been developed. Among these, the most commonly employed and effective approach is the addition of admixtures. Generally, these additives can be classified into Al-rich admixtures, cation exchange admixtures, nanoparticles, hydrophobic agents and other chemical admixtures.

1.1. Al-rich materials

Kani et al. [24] investigated the effect of Al-rich admixtures on the efflorescence of geopolymer binders, including metakaolin, slag and three types of calcium aluminate cement. They found that calcium aluminate cement is the most effective one to minimizing this issue. Maghsoodloorad et al. [15] also achieved success in reducing the efflorescence of alkali-activated phosphorus slag binder by Al-rich cement. Additionally, Zhang et al. [25] incorporated high aluminabased solid waste into alkali-activated steel slag. N-(A-)S-H gels were formed in the system, which presented enhanced absorption for alkali metal ions. A recent publication [26] revealed that the incorporation of sodium aluminate-activated water glass can mitigate the efflorescence of AAMs as well. The incorporation of soluble Al(OH)⁴ promoted the formation of more crosslinked C-(N-)A-S-H gels, which can bind more free Na⁺ ions in the pore solution.

1.2. Cation exchange agents

Wang et al. [27] found the inhibitory effects of 5 A zeolite on the efflorescence of AAS binder. They attributed this phenomenon to the exchange of Na $^+$ in the pore solution with Ca $^{2+}$ in the zeolite. This ion exchange led to a reduced concentration of Na $^+$ in the pore solution, effectively lowering the alkalinity of the pore solution and the efflorescence of AAS binders. Huang et al. [28] compared the efficiency of cation exchange between 5 A zeolite and vermiculite. They claimed that both chemicals can decrease the concentration of free Na $^+$ in AAS pastes, with 5 A zeolite showing a faster and stronger but lower exchange of Na than vermiculite.

1.3. Nanoparticles

Wang et al. [29] found that the addition of nano-silica results in the reduction in both pore volume and pore size diameter of the matrix, effectively alleviating the problem of efflorescence. Similarly, silica fume was recognized for its beneficial impact on microstructural refinement and permeability reduction, which has been confirmed to impede the problem of efflorescence [30]. Saludung et al. [31] also found the potential of silica fume in reducing efflorescence. However, they attributed this to the additional Si supplied by silica fume, which can bind more Na⁺.

1.4. Hydrophobic agents

Xue et al. [9] revealed that applying a silane surface modification to AAMs enhances the hydrophobicity of the surface. This treatment

substantially reduced the water absorption and moisture evaporation, which was effective in diminishing the leaching of alkali metal ions and the appearance of visual efflorescence. Other than surface treatment, Wu et al. [32] added caltite solution directly to AASF mortars. The filter membrane of alkaline stearate was generated by the reaction between caltite and alkaline activators, which contributed to minimizing the leaching of Na⁺ and efflorescence of materials. Pasupathy et al. [33] coated the sand with two hydrophobic agents and also achieved success in efflorescence mitigation.

Moreover, researchers have also identified the addition of calcium hydroxide [34] and rice husk ash [35] can mitigate the efflorescence of AAS pastes and mortars. In summary, all the aforementioned mitigation methods focus on the paste or binder modifications using additives or admixtures, neglecting the role of aggregates. However, aggregates constitute 60–80 % of concrete volume in real constructions, making it promising to address this issue at scales. Conventional fine aggregates (e. g., river sand [36], sea sand [37] or manufactured sand [38]) are predominantly composed of quartz, which is highly crystalline and chemically inert under high alkalinity. Consequently, developing chemically reactive aggregates under alkaline conditions is essential.

Lightweight fine aggregates (LWFA) are manufactured by sintering selected clay, shale or fly ash, followed by rapid cooling treatment. These kinds of aggregates consist of amorphous SiO2 and Al2O3, which can react with portlandite and show pozzolanic reactivity in cementitious materials [39,40]. Besides, due to the porous structure of LWFA, it can also serve as an internal curing agent to promote cement hydration and reduce self-desiccation [41,42]. Additionally, LWFA and lightweight aggregates (LWA) have also been incorporated into AAMs [43–49]. Zheng et al. [46] found that the pre-wetted LWA enhances the cracking resistance of AAS concretes. Chen et al. [49] investigated the mechanical properties of geopolymer concretes blended with fly ash ceramsite, shale ceramsite and clay ceramsite, respectively. They found that the concrete with fly ash ceramsite exhibited the highest compressive strength. Additionally, the strength development of LWAbased geopolymer subjected to sulfuric acid [50] and the micromechanical characteristics of the interfacial transition zone between lightweight iron-rich aggregates and AAS pastes [48] were reported as well. Accordingly, most of the previous studies have concentrated on the effect of LWA or LWFA on the mechanical properties of AAMs. However, the impact of them on the durability of AAMs remains unknown. Given these specific physicochemical properties of LWFA, it is intriguing to explore its impact on the chemical properties of AAMs and its potential to mitigate efflorescence.

In this study, AAS mortars were prepared using slag as the sole precursor and NaOH (NH) solutions as activators, with aluminosilicate LWFA partially replacing sand at volumetric substitution levels of 0 %, 20 %, and 50 %. Efflorescence was observed under controlled conditions, with the bottoms of the cylindrical mortars in contact with water. Leaching tests were conducted to assess Na leachability from both pore solutions and gels. Additionally, the dissolution behaviour of various ions from LWFA in alkali activators was examined. Finally, the impact of LWFA on the pore solution, reaction products, gel structure, paste chemistry, pore structure, and mechanical strengths (compressive and flexural) was analyzed. The mitigation mechanisms of LWFA on the efflorescence of AAS mortars were revealed from the aspects of gels, pore solution and microstructure. The potential for LWFA application in AAMs was also critically assessed.

2. Materials and methods

2.1. Raw materials

The chemical composition of slag measured by X-ray fluorescence (XRF) is shown in Table 1. The particle size of slag ranged from 0.5 to 50 μm , with a d_{50} of 18 μm . The standard sand (EN 196–1) and LWFA with particle sizes between 0 and 4 mm were used. The chemical composition

Table 1
Chemical composition of slag and LWFA. (wt%).

	CaO	Al_2O_3	SiO_2	MgO	Fe_2O_3	K ₂ O	Na_2O	${ m TiO_2}$	Other
Slag	46.8	9.0	33.2	7.3	0.6	0.3	0.3	0.7	1.8
LWFA	3.8	18.4	58.2	3.8	9	3.4	1.2	1.1	1.1

of LWFA is presented in Table 1 and its appearance is shown in Fig. A1. Fig. 1 shows the mineralogical composition of LWFA determined by Xray diffraction (XRD). Quartz (SiO₂) and hercynite (FeAl₂O₄) were the two main crystal phases in LWFA. Besides, a small hump ranging from 20° to 35° suggested the presence of amorphous phases. Fig. 2 shows the pore volume and pore size distribution of LWFA determined by mercury intrusion porosimetry (MIP). The total pore volume of LWFA was around 49 %, with the pores primarily distributed across two size ranges: $0.1-10 \mu m$ and $> 100 \mu m$. The extrusion curve indicated a significant volume of ink-bottle pores in LWFA, which contributed to its excellent water retention properties. The saturated water absorption of LWFA was approximately 14 % by mass. The bulk density of sand and LWFA was 2600 kg/m³ and 1530 kg/m³, respectively. Given that efflorescence tends to occur more rapidly in materials with a porous structure [7], a NH solution was used as the alkali activator. The use of NH solution also provided a simplified AAS system, allowing for a focused analysis of the effects of LWFA without interference from other anions, such as silicate, carbonate or sulfate, which are often present in alkali activators. The NH solution was prepared through the combination of commercial sodium hydroxide solution (50 wt%) and deionized water.

2.2. Mortar preparation

The mixture design of AAS mortars is presented in Table 2. The alkali dosage (Na₂O in activators/slag) was 5 %. The volume of fine aggregate, comprising sand and LWFA, constituted 55 % of the mixture. The percentage in the label referred to the content of LWFA by volume of total fine aggregate. For instance, "LWFA_20%" means that 20 % volume of the fine aggregate in AAS mortars is occupied by LWFA. Prior to casting, dry LWFA was immersed in water for 1 d to prevent excessive water absorption during the mixing, which could otherwise affect the workability of fresh mortars [51–53]. After 1 d of water immersion, the wet LWFA was surface-dried using a towel. The slag, sand and wet LWFA were mixed by a Hobart mixer for 1 min at a slow rate. Then, the NH solution was poured into the mixing bowl, followed by 1 min of slow mixing and 1 min of fast mixing. The fresh mortar was moulded in

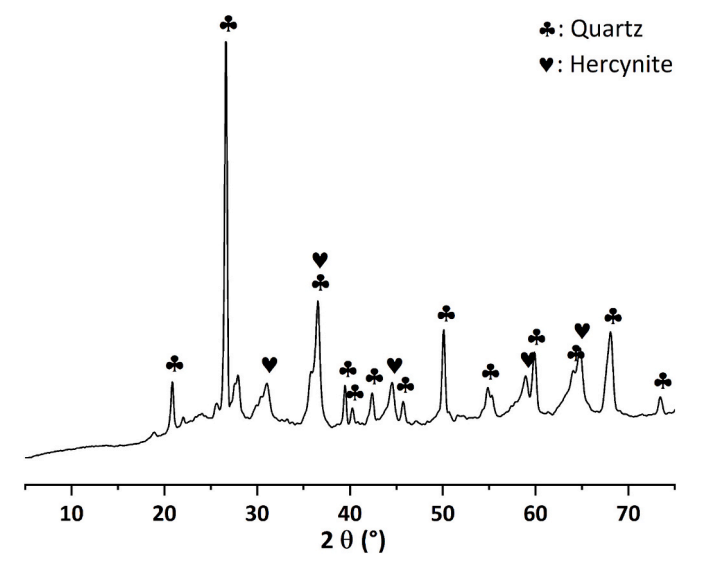


Fig. 1. Mineralogical composition of LWFA determined by XRD.

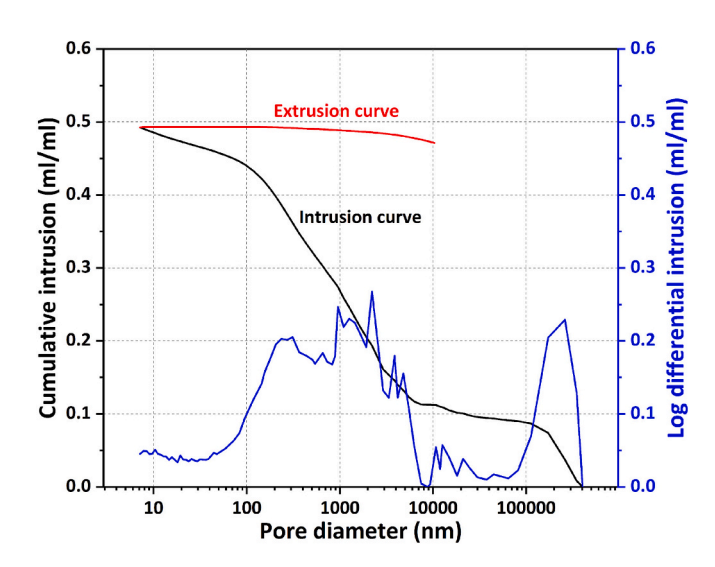


Fig. 2. Pore volume and pore size distribution of LWFA determined by MIP.

Table 2Mixture design of AAS mortars.

	Slag (g)	Sand (g)	Dry LWFA (g)	Activator (g)	w/b
LWFA_0%	1000	2500	0	554.6	0.505
LWFA_20%	1000	2000	294.2	554.6	0.505
LWFA_50%	1000	1250	735.6	554.6	0.505

w/b: water/binder ratio

polyethene bottles (ϕ 35 mm \times 70 mm) and 4 cm \times 4 cm \times 16 cm prismatic moulds for further measurements. The densities of the three mortars sealed for 28 d were measured, resulting in values of 2191.4 kg/m³, 2080 kg/m³ and 1928.4 kg/m³, respectively.

2.3. Efflorescence and leaching tests

2.3.1. Efflorescence tests

The fresh mortars contained in polyethene bottles (ϕ 35 mm \times 70 mm) were sealed for 28 d and then cut into cylinders with a height of 50 mm. The cutting side of each cylinder was immersed in deionized water to a depth of 10 ± 1 mm within a glassy dish. This method was widely used in previous work to obtain efflorescence in a short period [7,8]. The cylinders were exposed to ambient conditions ($T=20\,^{\circ}$ C and RH = 55%) for 28 d. Three replicates were conducted for each mixture.

2.3.2. Leaching tests

To quantify the efflorescence of AAS mortars, Na in the leachate of efflorescence products was measured. The cylinders after efflorescence were immersed in 150 ml of deionized water and were cleaned ultrasonically for 30 s to remove the efflorescence products [54]. The concentration of Na in the resulting solution was measured using a PerkinElmer Optima 5300DV ICP-OES spectrometer. The Na amount in the efflorescence product per cylinder was calculated based on this concentration [54].

Moreover, leaching tests were also conducted using both fresh mortar pieces and dried mortar powders. The tests with mortar pieces aimed to evaluate the leaching stability of Na in fresh AAS mortar

(mostly pore solution), while the tests with powdered samples focused on the leaching stability of Na in C-(N-)A-S-H gels. For mortar pieces, the AAS mortars sealed for 28 d were crushed into 4-6 mm pieces and 10.00 g (\pm 0.01 g) of pieces were immersed in 100.0 g (\pm 0.1 g) deionized water for 28 d, and Na concentration in the leachate was measured. For powdered samples, the AAS mortars sealed for 28 d were crushed into powder in isopropanol to stop the reaction. Then, the powder was treated with ether and dried in a vacuum oven. 1.000 g (\pm 0.005 g) powder sample was immersed in 50.0 g (\pm 0.1 g) deionized water for 28 d, and the Na concentration in the leachate was measured. Additionally, to evaluate the pozzolanic reactivity of LWFA, the leaching test of sand and LWFA subjected to NH activators immersion was conducted. The aggregate/liquid ratio followed that specified in Table 2. The concentration of Na, Si, Al and Ca was measured by ICP-OES, while the concentration of OH- ions in the leachate was obtained by titration tests using a 0.1 mol/l HCl solution.

2.4. Other characterizations

2.4.1. ICP-OES, XRD, TGA and FTIR

The pore solution of 28 d sealed AAS mortar was extracted by the steel-die method, as described in [55]. Then, the ion concentrations of Na, Al, Si and Ca in the pore solution were measured by ICP-OES, and the concentration of OH ions was determined through titration as mentioned above. XRD analysis was carried out to determine the phase assemblage of efflorescence products and AAS mortars. A Bruker D8 Advance diffractometer with CuKa (1.54 Å) radiation was used, with detection angles ranging from 5° to 75°, a step size of 0.02° and a swell time of 5 s per step. The efflorescence products were obtained from the white deposits on AAS cylinders after 28 d of exposure. The powdered samples measured in XRD as well as the following tests were the same as those used in the leaching test of 28 d AAS mortar samples. Thermogravimetry analysis (TGA) was performed using a NETZCH TG-449-F3-Jupiter instrument to assess the thermal stability and decomposition behaviour of the samples. Powdered samples were subjected to heating from 40 °C to 1000 °C at a rate of 10 °C/min under an argon atmosphere. Fourier-transform infrared spectroscopy (FTIR) analysis was conducted on a Spectrum TM 100 Optical ATR-FTIR spectrometer. Spectral measurements were taken from 600 cm⁻¹ to 4000 cm⁻¹ with a resolution of 4 cm^{-1} .

2.4.2. SEM and EDX

An FEI QUANTA FEG 650 scanning electron microscope (SEM) with a solid-state energy dispersive X-ray spectroscopy (EDX) detector was employed to observe the morphology and characterize the elemental composition of pastes around sand and LWFA. Bulk AAS mortars, sealed for 28 d, were first immersed in isopropanol for 7 d to stop the reaction, followed by being dried in a vacuum oven. Then, the dried sample was impregnated with low-viscosity epoxy resin. After the epoxy was dried, the sample was polished with sandpaper and cloth with diamond pastes, followed by carbon coating to enhance the conductivity and improve imaging quality. The samples were examined under backscattering electron (BSE) mode at an acceleration voltage of 15 kV and a working distance of 10 mm, all under high-vacuum conditions.

2.4.3. MIP and sorptivity tests

The pore structure of AAS mortars was evaluated using MIP analysis and a modified capillary sorptivity test. MIP analysis was used to determine the total porosity of AAS mortars at dry state, while the modified sorptivity test assessed the water absorption capacity before efflorescence testing. The reaction-arrested and dried mortar pieces (approximately 4–6 mm in size) were utilized to conduct MIP tests using a Micrometrics PoreSizer 9500. The test comprised three steps: mercury intrusion at low pressure ranging from 0 to 0.170 Mpa, mercury intrusion at high pressure ranging from 0.170 to 210 Mpa, and mercury extrusion. This enabled the detection and characterization of pores

spanning from 400 µm down to 7 nm. A modified sorptivity test was conducted based on cylindrical mortars with dimensions of φ 55 mm \times 50 mm. Unlike the standard sorptivity test in ASTM C1585–13 [56], in which the samples are dried before testing [57], in this study, the samples were tested directly after 28 d of sealed curing without preconditioning. The side and top of the cylinders were covered by aluminium taps while the bottom of the samples was immersed in deionized water to a depth of 10 mm (\pm 1 mm). Mass changes were recorded at specific testing intervals of 5 min, 10 min, 20 min, 30 min, 1 h, 6 h, 1 d, 3 d, 4 d, 5 d, 6 d, and 7 d. Three replicates were measured for each group. The water sorptivity I (mm/s $^{1/2}$) of specimens was calculated using Eq. 1:

$$I = \frac{m_t}{a \times \rho} \tag{1}$$

where m_t (g) is the mass of samples at moment t, a (mm²) is the exposed area of the specimen, ρ (10⁻³ g/mm³) is the density of water.

2.4.4. Flexural and compressive strength testing

Flexural and compressive strengths of AAS mortars were measured to study the effect of LWFA substitution on the mechanical properties of mortars. The 4 cm \times 4 cm \times 16 cm samples were sealed for 7 d before being exposed to ambient conditions up to 28 d. Strength measurements were conducted at 7 d and 28 d. The testing procedures and loading parameters were according to NEN-EN 196–1 [58].

3. Results

3.1. Efflorescence tests

3.1.1. In-situ observation

As shown in Fig. 3, the efflorescence on AAS cylinders accumulates with time. The mortars without LWFA showed more serious efflorescence at early ages (1 d and 7 d). Normally, efflorescence products mainly consist of sodium (bi)carbonates, with Na primarily sourced from the pore solution. Both a higher Na concentration in the pore solution and a porous microstructure can increase the supply of Na and enhance the efflorescence potential of materials [14,59]. In addition to Na⁺, OH⁻ also significantly influences the formation of efflorescence products. As reported in [60], gaseous $CO_{2(aq)}$ dissolved in water to form $H_2CO_{3(aq)}$, which remained stable under neutral conditions. However, in the presence of OH⁻, $H_2CO_{3(aq)}$ became unstable and hydrolysed to $HCO_{3(aq)}$ and $CO_{3(aq)}^{2-}$ to different extents, depending on the pH level [60]. Therefore, the reduced efflorescence of AAS mortar with LWFA was probably attributed to a decreased supply of Na⁺ and OH⁻.

After 28 d of exposure, AAS mortars containing LWFA also showed less efflorescence than those without LWFA. This effect was more pronounced in mortars with a higher LWFA content (LWFA_50%). Additionally, the efflorescence front (marked by dark green/blue traces) of the cylinders of "LWFA_20%" and "LWFA_50%" is lower than that of "LWFA_0%", as shown in Fig. 4. As stated in [54], the efflorescence front was correlated with the porosity of materials: lower porosity resulted in a lower efflorescence front. However, this statement appeared inconsistent with the MIP results (Fig. 14), which reveal that LWFA-containing mortars actually possessed higher porosity than LWFA-free mortars. This discrepancy suggested the involvement of additional mechanisms beyond porosity alone. Further insights are provided by water absorption results (Fig. 15). Overall, the observation in this section indicated the excellent efficacy of LWFA in mitigating efflorescence.

3.1.2. Efflorescence products

Fig. 5 shows the phase assemblage of efflorescence products on the mortar cylinders. Thermonatrite ($Na_2CO_3 \bullet H_2O$) was identified as the main phase in the efflorescence product of three mortar samples. This suggested that the substitution of LWFA shows a limited impact on the



Fig. 3. Visual observation of the efflorescence of AAS mortar cylinders with time.

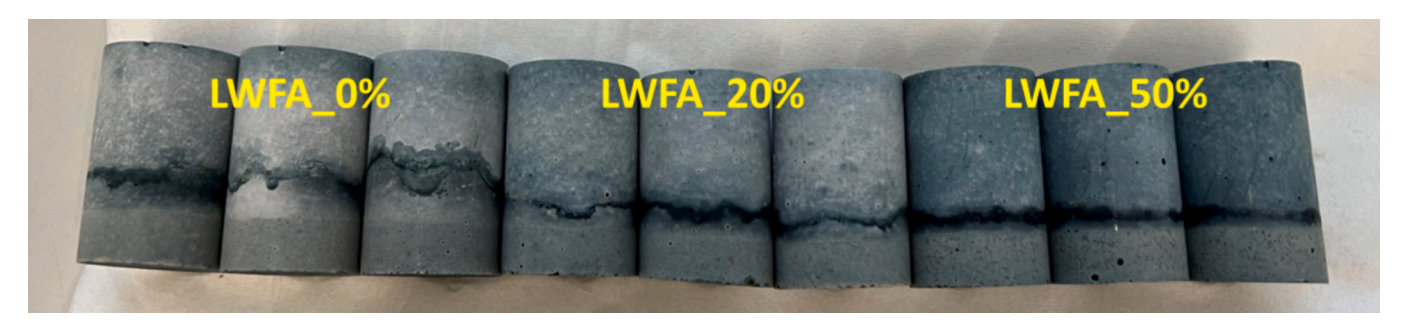


Fig. 4. Ultrasonically cleaned AAS mortar cylinders after 28 d of efflorescence. From left to right, three cylinders as a group refer to "LWFA_0%", "LWFA_20%" and "LWFA_50%", respectively. The darker green/blue trace indicates the "efflorescence front" of AAS cylinders. (For interpretation of the references to colour in this figure legend, the reader is referred to the web version of this article.)

phase assemblage of efflorescence products. Traces of quartz were also identified in the LWFA_0% and LWFA_20% groups, likely originating from sand or LWFA during the scraping of efflorescence products. As reported in [54], the primary efflorescence product of NH pastes was sodium carbonate heptahydrate ($Na_2CO_3 \bullet 7H_2O$). The appearance of thermonatrite instead indicated reduced hydrated water in the

efflorescence product of the mortar sample. Typically, the presence of sand has two effects on the system. On one hand, sand is considered impermeable, and its introduction can densify the material. On the other hand, sand introduces interfaces with the paste, which have high water/binder ratios and are generally more porous than the matrix [42]. In this study, the densifying effect of sand appeared to be more significant than

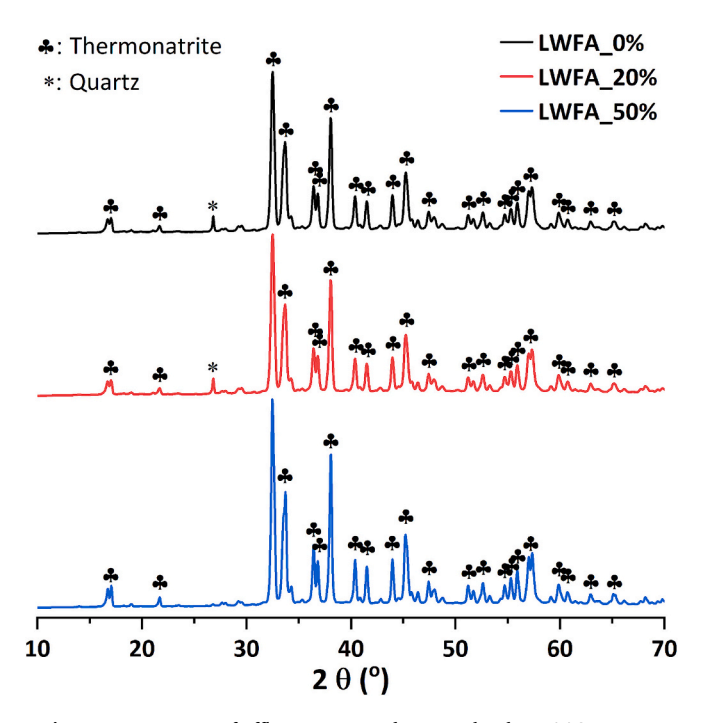


Fig. 5. XRD pattern of efflorescence products on the three AAS mortars.

its impact on increasing porosity. The incorporation of sand might reduce water transport within the material, thereby lowering the content of hydrated water in the efflorescence products.

3.2. Leaching tests

3.2.1. Leaching of efflorescence products

Visual observation has inherent limitations on the quantification of efflorescence of AAS mortars, as it overlooks factors such as the thickness and density of efflorescence products. In this study, a quantification method was used by determining the amount of Na in efflorescence products [54]. Following this method, the amount of Na in efflorescence products per cylinder can be quantified, which is shown in Fig. 6. As

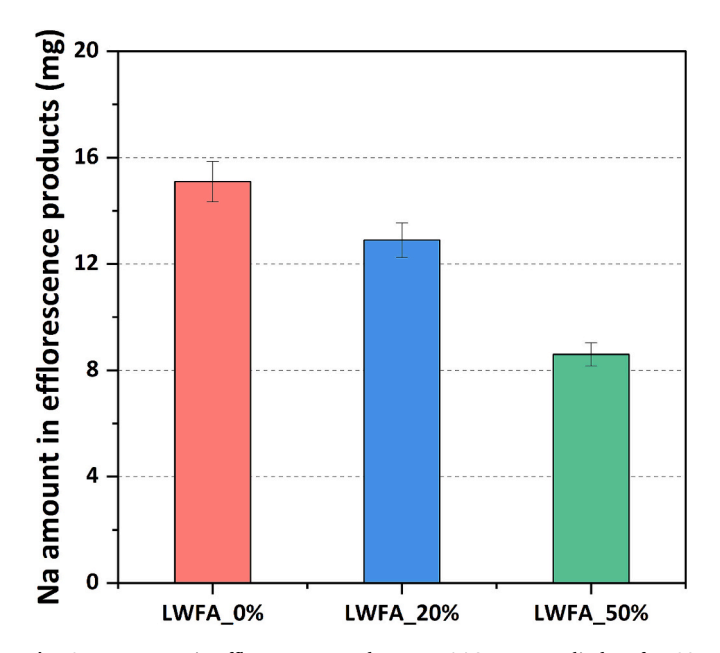


Fig. 6. Na amount in efflorescence products per AAS mortar cylinder after 28 d of exposure.

demonstrated in [54], the Na amount in the efflorescence product of NH pastes, with the same dimensions as those used in this work, was 118 mg per cylinder. This indicated that the efflorescence of AAS pastes is more severe than that of AAS mortars. The addition of fine aggregates can efficiently lower efflorescence [59], due to a lower content of $\rm Na^+$ and $\rm OH^-$ within the same volume than pastes. Additionally, compared to the reference mortar, LWFA substitutions of 20 % and 50 % resulted in efflorescence reduction of 14.6 % and 43 %, respectively.

3.2.2. Leaching of AAS mortar pieces and powders

Given the lower density of LWFA-based mortars than normal mortars (section 2.2), it was rational to compare the leaching result by volume. Therefore, we normalized the leaching results by volume, as depicted in Fig. 7A. The Na concentration in the leachate decreased as LWFA dosages increased, indicating that the presence of LWFA hindered the leaching of Na. Generally, Na in mortars can be categorized into three types: free Na⁺ in the pore solution, weakly bonded Na in C-(N-)A-S-H gels and strongly bonded Na in C-(N-)A-S-H gels [5,59]. Free Na is related to the alkalinity of the pore solution, while weakly and strongly bonded Na are incorporated into the C-(N-)A-S-H gels. Given the use of fresh AAS mortar pieces, it is plausible that free Na in the pore solution may contribute significantly to the leaching results.

Fig. 7B shows the Na concentration in the leachate of powdered mortars. As mentioned in section 2.3, the reaction of powdered samples was arrested in isopropanol, meaning that all Na in the leachate originated from C-(N-)A-S-H gels. It is interesting to observe that the Na concentration in the leachate increased with the LWFA dosage, contrary to the trend observed for mortar pieces (Fig. 7A). According to [5,55,61], Na⁺ is the predominant ion leached from synthesized C-(N-) A-S-H gels subjected to water immersion due to its weak bonding in the interlayer of gels. Besides, the leaching amount of Na increases with its initial content in the gel, implying that the gels in mortars with LWFA have a higher Na uptake. As reported in [5], the gel with a lower Ca/Si ratio and a higher Al/Si ratio shows a higher Na/(Al + Si) ratio due to enhanced charge negativity on gel substrates. This suggested that the addition of LWFA may alter the gel chemistry, potentially enhancing the Na uptake by the gels.

3.2.3. Leaching of aggregates in the activator

Fig. 8 shows the ion concentrations of Na, OH, Si, Al and Ca in the leachate of LWFA after immersion in the NH activator for 28 d. The solution was dominated by Na⁺ and OH⁻, with the concentration of OH⁻ slightly lower than that of Na⁺. After 28 d of immersion, the concentrations of Na+ and OH- decreased slightly compared to the initial activator, with a more significant reduction observed in solutions with a higher LWFA content. This suggested that the pozzolanic reaction of LWFA reduces the alkalinity of the solution. Simultaneously, Si and Al species were dissolved from the structure of LWFA. The solution with a higher content of LWFA showed a higher concentration of Si and Al. Interestingly, although the sand was generally considered inert, it can also release some amount of Si and even Al under alkaline conditions. However, the quantities released from sand were considerably lower than those from LWFA. The concentration of Ca remained relatively low compared to the other elements and showed little variation between them. Overall, these dissolution tests of aggregates indicated the pozzolanic reactivity of LWFA, which can supply extra Si and Al to the

3.3. Impacts of LWFA on AAS mortars

3.3.1. Pore solution

The ion concentration of Na, OH, Si, Al and Ca in the pore solution of AAS mortars sealed for 28 d is shown in Fig. 9. Similar to Fig. 8, Na $^+$ and OH $^-$ dominated the pore solution, but their concentrations were lower, primarily due to the reaction of slag and the formation of C-(N-)A-S-H gels. Additionally, it was observed that both Na and OH concentrations

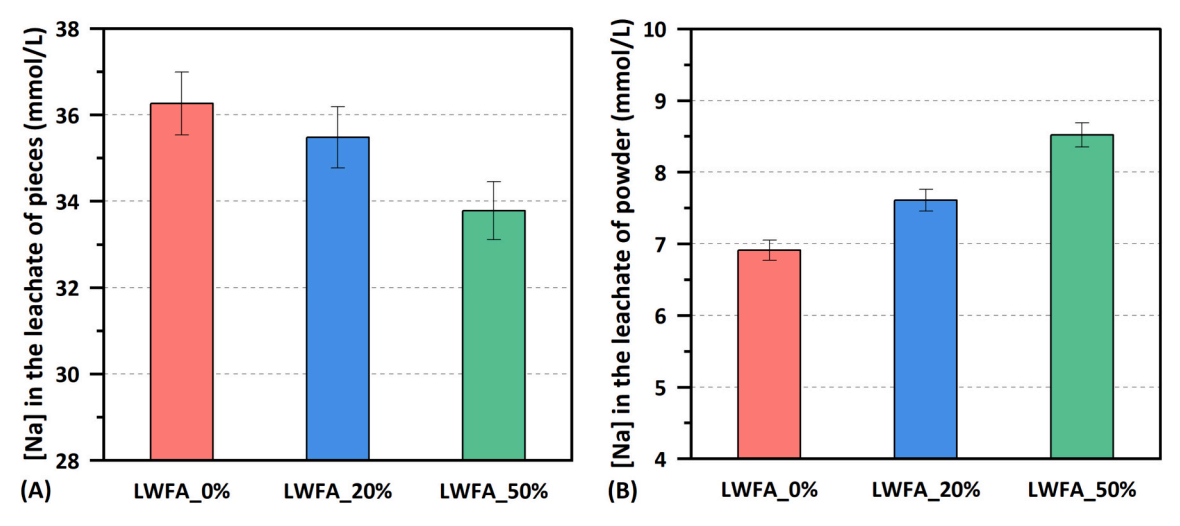


Fig. 7. Na concentrations in the leachate of AAS mortar pieces and powders. [Na] refers to the concentration of sodium.

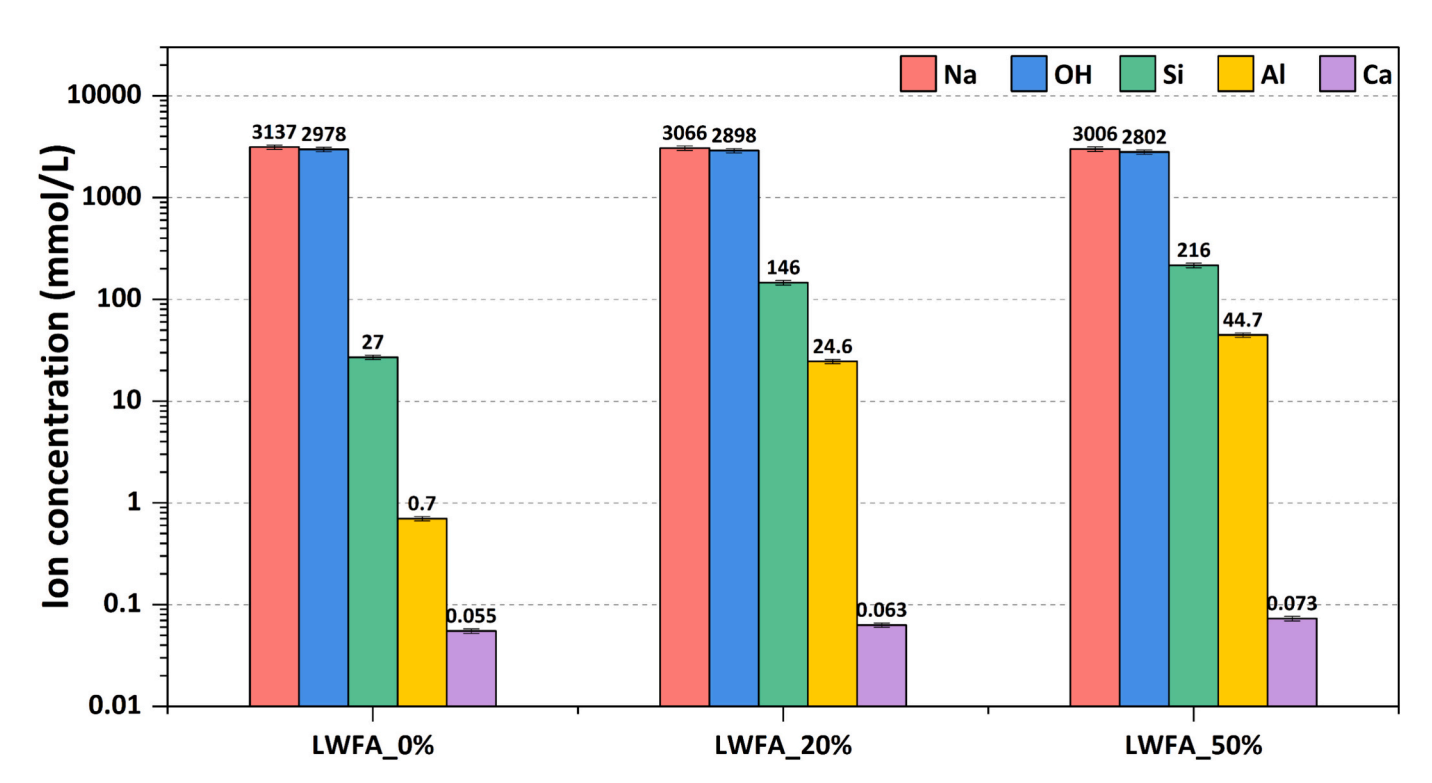


Fig. 8. Ion concentration of Na, OH, Si, Al and Ca in the leachate of LWFA subjected to immersion of the NaOH activator for 28 d. The concentration of Na⁺ and OH⁻ of the fresh NH activator is 3297 and 3271 mmol/L, respectively.

decrease with the increase in LWFA dosage. Specifically, substituting 20 % and 50 % LWFA reduced the concentration of Na $^+$ by 7.7 % and 15.5 % and the concentration of OH by 8.3 % and 10.4 %, respectively. These decreases can be attributed to the pozzolanic effect of LWFA, as well as the introduction of extra water by the pre-moistened LWFA. The concentration of Si increased with the increase of LWFA dosage, attributed to the dissolution of extra Si species from LWFA (Fig. 8). The concentrations of Al were comparable across three pore solutions, with the two LWFA mortars exhibiting slightly higher values than the reference. The concentration of Ca remained relatively low compared to the other ions, due to a low solubility of Ca under high alkalinity conditions.

3.3.2. Reaction products

Fig. 10 shows the XRD, TGA and FTIR results for AAS mortars. As shown in Fig. 10 A, the XRD pattern is dominated by quartz, the main

phase in both sand and LWFA. The intensity of the quartz signal decreased with the LWFA dosage increases, which probably indicated a higher content of quartz in sand than LWFA. The characteristic peak of gels can be observed near 30°, but the intensity was too low to discern any difference among the three mortars, due to the high content and crystallinity of quartz masking the signal. Fig. 10B shows the TG and DTG curves of AAS mortars. The total weight loss of samples increased with higher LWFA dosage, which indicated an increasing content of reaction products. The DTG curves were mainly dominated by two peaks: the first corresponds to the weight loss of C-(N-)A-S-H gels between 40 and 250 °C and the second to hydrotalcite-like (ht) phases between 300 and 400 °C. The weight loss of hydrotalcite in the three mortars appeared to be comparable, while that of the gels showed some distinctions. The sample with a higher LWFA content showed a higher weight loss of gels. Typically, the weight loss in gels is mainly due to the

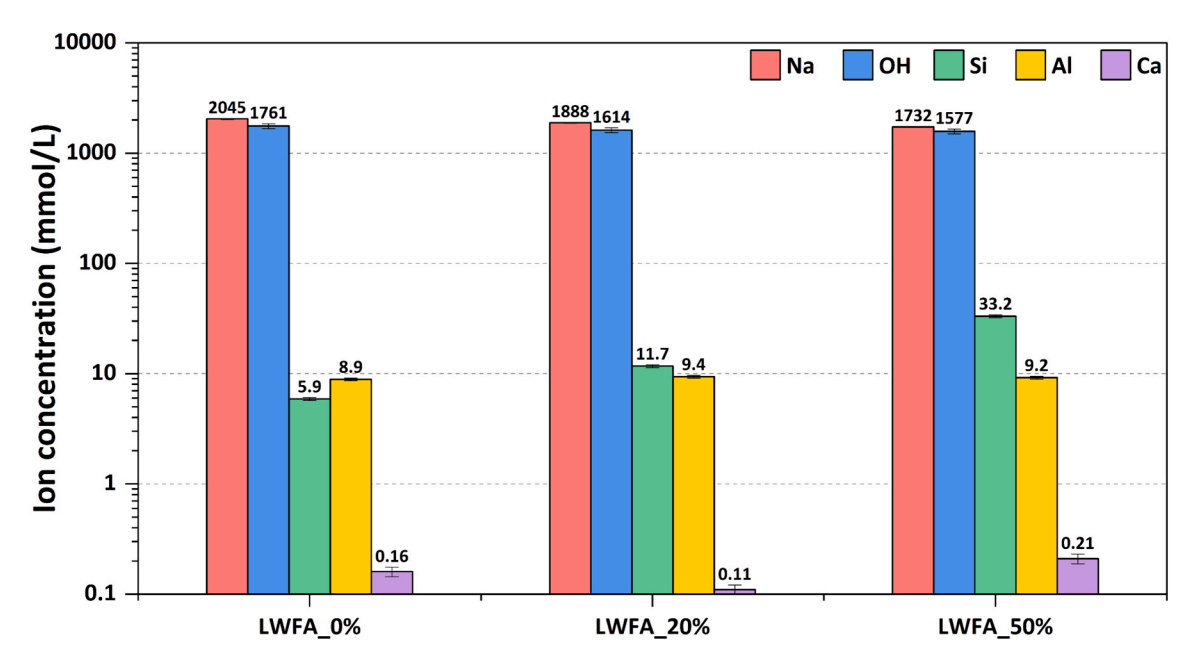


Fig. 9. Ion concentrations of Na, OH, Si, Al and Ca in the pore solution of AAS mortars sealed for 28 d.

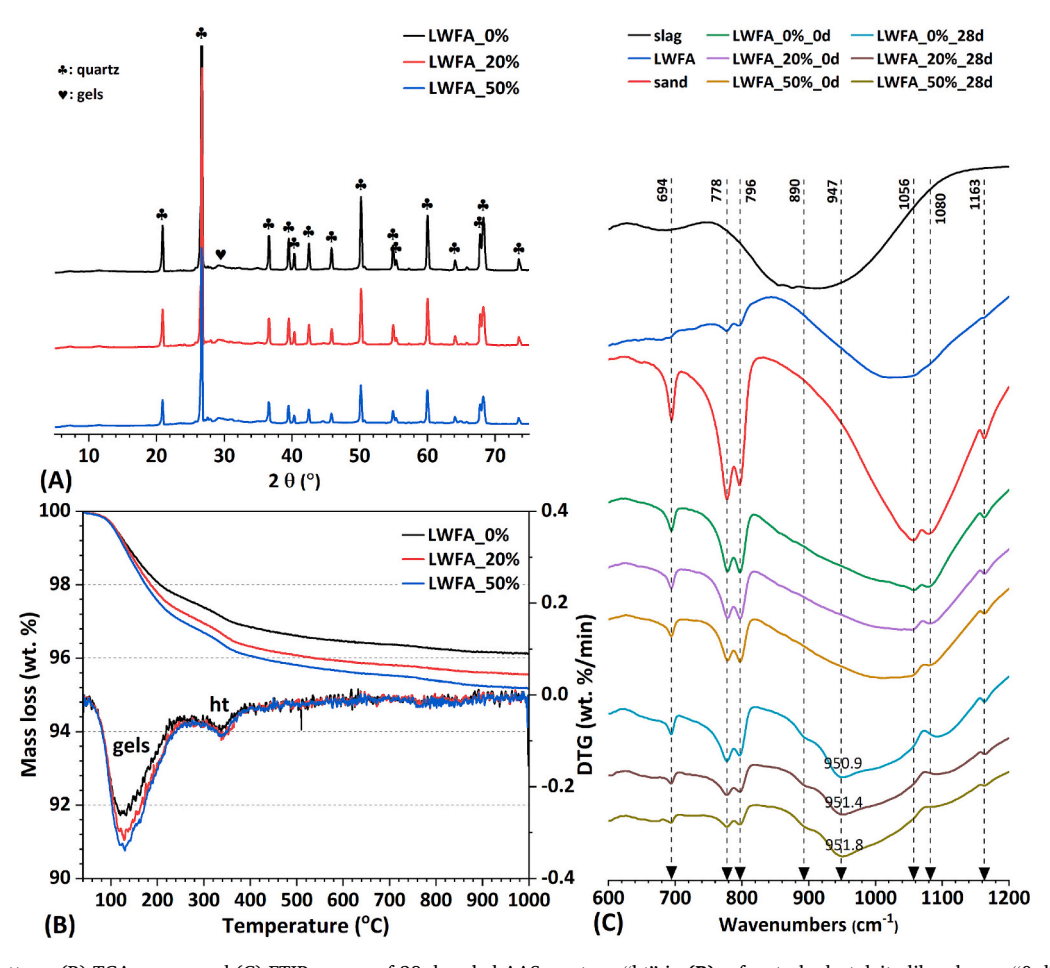


Fig. 10. (A) XRD pattern, (B) TGA curves and (C) FTIR curves of 28 d sealed AAS mortars. "ht" in (B) refers to hydrotalcite-like phases. "0 d" in the label of (C) indicates the raw material consisting of unreacted slag, sand and LWFA.

chemically bonded or physically absorbed water, which is closely related to the amount and chemistry of gels as well as the drying method. In this study, the drying of powdered samples strictly followed

the standard [62], ensuring that the free water or physically absorbed water was consistent across samples. Hence, this discrepancy can be attributed to a higher content of gels in the LWFA-blended mortar. As

shown in Fig. 8, Si and Al species can be dissolved from LWFA during the immersion of the alkali activator. These ions can serve as the raw materials for the formation of gels. Besides, the internal curing effect of LWFA can provide the matrix with a high-humidity condition, which contributes to the reaction of slag and the formation of gels as well. Furthermore, as reported in [63], the gel with a higher content of alkali metal ions contains a higher content of chemically bound water. Therefore, a higher weight loss of gels in LWFA-blended mortars was attributed to a higher content of Na in gels. This was partially consistent with the leaching test results of powdered AAS mortars (Fig. 7B).

Fig. 10C shows the results of FTIR analysis of slag, sand, LWFA and AAS mortars. There are no sharp absorption peaks but rather broad humps in slag and LWFA. Considering that both slag and LWFA are silicate materials, a higher wavenumber of the hump of LWFA indicated a more crosslinked structure. This is consistent with the NMR results in [51,64], where the chemical environment of Si in slag is dominated by Q⁰ and Q¹, while LWFA is Q³ and Q⁴, indicating a significantly higher reactivity of slag. The main hump of sand showed even higher wavenumbers than LWFA, suggesting a more crosslinked network and consequently lower reactivity. Therefore, LWFA can dissolve more Si than sand. The peaks located at 694 cm⁻¹, 778 cm⁻¹, 796 cm⁻¹, 1056 cm⁻¹, 1080 cm⁻¹ and 1163 cm⁻¹ in the infrared pattern of sand are assigned to the vibration of Si-O-Si in quartz [65]. The spectra of "LWFA_0%_0d", "LWFA_20%_0d" and "LWFA_50%_0d" represented combinations of raw materials in three mixtures, showing minimal differences among them. However, after 28 d of reaction, a newly formed hump ranging from 850 cm⁻¹ to 1100 cm⁻¹ was observed in all three mortars. According to [66], the peak near 950 cm⁻¹ corresponds to the asymmetrical stretching vibration of Si-O-Si(Al) in Q² units of gels, and a small shoulder at the lower frequency of the hump (890 cm⁻¹) is assigned to the bending vibration of Si-O in gels. Furthermore, the average peak wavenumber of Q² units in the three mortars was 950.9, 951.4 and 951.8 cm⁻¹, respectively. This slight variation indicated that the gel in the system with a higher dosage of LWFA shows a higher degree of polymerization, primarily attributed to the presence of extra Si and Al dissolved from LWFA.

3.3.3. Mortar morphology and paste chemistry

Fig. 11 shows the typical morphology of pastes around sand and LWFA. The interface between sand and pastes is distinct, with the paste

surrounding the sand appearing coarser than the matrix. In contrast, the interface between LWFA and pastes was less evident, and the paste surrounding LWFA appeared denser than that around the sand. This difference can be explained by the capillary effect [67]. The water/ binder ratio of pastes around normal aggregates is typically higher than that of the matrix, resulting in a more porous pore structure [68]. Due to the porous structure and pre-absorbed water, the capillary effect of LWFA is more evident than sand. However, unlike sand, LWFA shows reactivity under alkali conditions [69,70], which leads to the release of extra Si and Al species. These species react with Ca and Na in the pore solution, contributing to the formation of gels and the densification of surrounding pastes. This statement was supported by the higher water loss in the gels of LWFA blended mortars as shown in the DTG curve (Fig. 10B). As reported in [71], the interfacial transition zone (ITZ) in normal concrete is thicker than that in LWFA-blended concrete. The impact of LWFA on the microstructure of AAS pastes will be further discussed in the pore structure sections.

Fig. 12 A shows the Si/Ca versus Al/Ca ratios of the pastes around sand and LWFA. In general, the Si/Ca ratio of the paste around LWFA ranged from 0.6 to 1.0, which was higher than that around sand (0.4–0.9). Besides, the Al/Ca ratio of the paste around LWFA was higher than that around sand as well. As indicated by the arrow in Fig. 12 A, the paste around LWFA contains more Si and Al. This can be ascribed to the additional Si and Al supplied by LWFA (Fig. 8). Fig. 13B shows the Al/Si versus Mg/Si ratios of the pastes around sand and LWFA. There was a positive linear correlation between the Al/Si and Mg/Si ratios, despite some irregular data points. As noted in [72], such a linear correlation between the Mg/Si and Al/Si ratios typically suggests the presence of hydrotalcite-like phases. The positive X-axis intercept indicates the extent of Al incorporation of C-S-H gels in the rim of slag, while the slope of the trendline shows the Mg/Al ratio of hydrotalcite. In both groups, the Al/Si ratio of gels in the rim and the Mg/Al ratio of hydrotalcite were comparable in the pastes around sand and LWFA, as they were mainly determined by the chemical composition of the slag.

Fig. 13 shows the box plot of different elemental ratios in the paste around sand and LWFA. Consistent with the result in Fig. 12 A, the paste around LWFA showed a lower Ca/(Si + Al) ratio than that around sand (Fig. 13A). In contrast, the paste around LWFA showed a higher Na/(Si + Al) ratio than that around sand (Fig. 13B). This indicated a higher uptake of Na in the paste with the incorporation of LWFA, which agreed

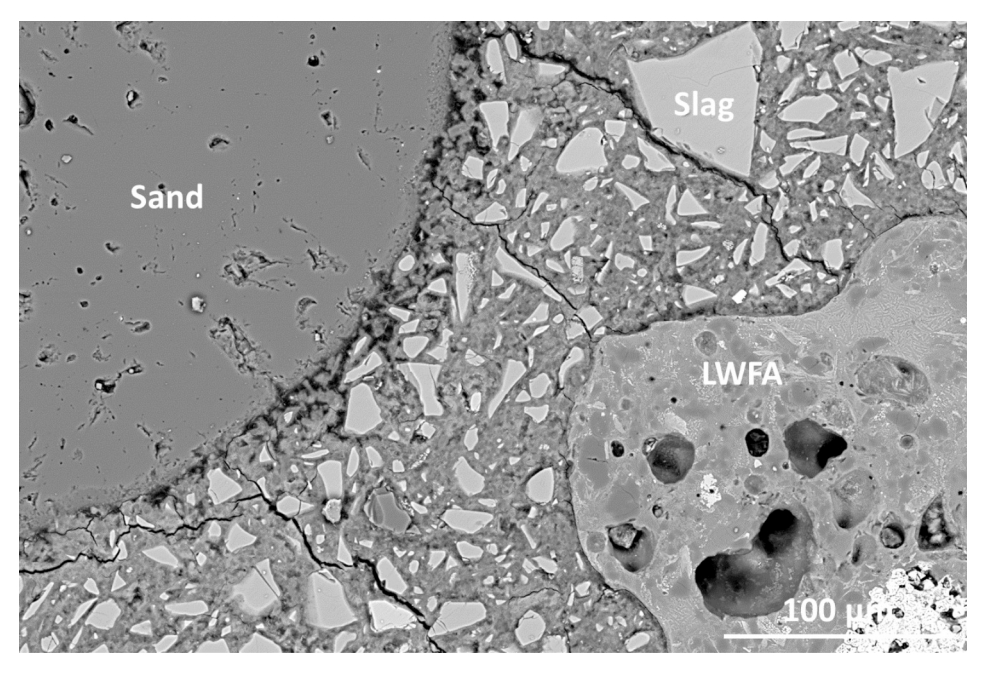


Fig. 11. Typical morphology of pastes around sand and LWFA. The cracks in the matrix can be attributed to the sample crushing and polishing processes.

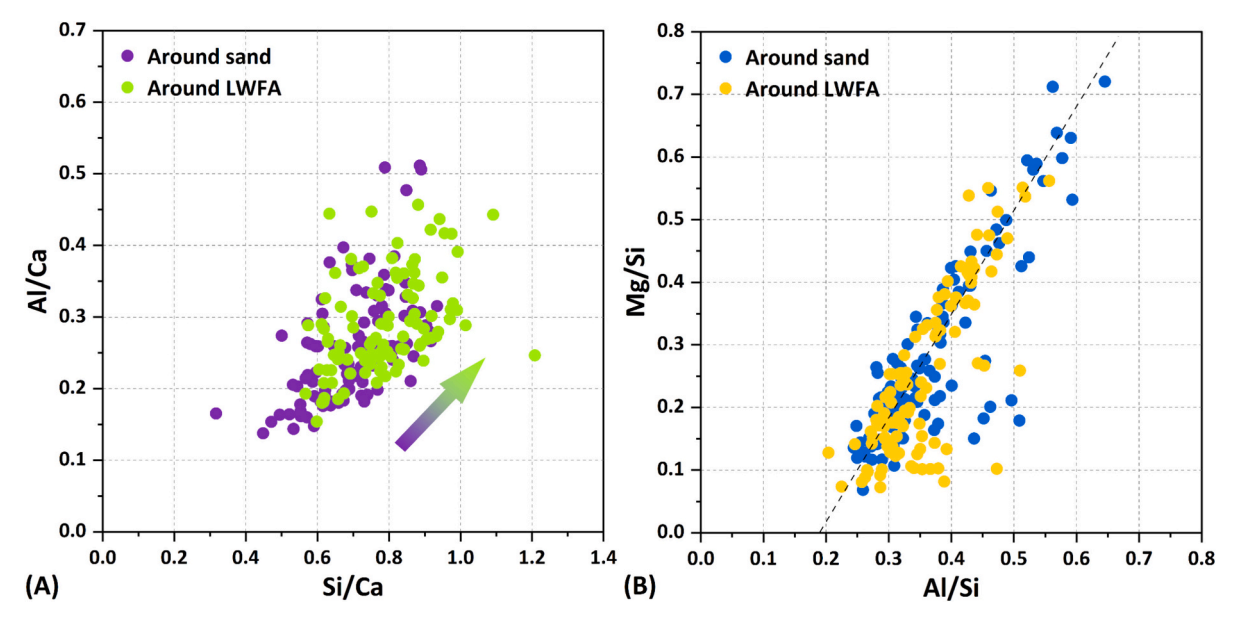


Fig. 12. (A) Si/Ca versus Al/Ca ratios and (B) Al/Si versus Mg/Si ratios of the pastes around sand and LWFA. The arrow in (A) indicates the variation of the data point of the paste around the aggregate from sand and LWFA.

with the leaching results of powdered mortar (Fig. 7B). Fig. 13C shows the Mg/Al ratio of the paste. Mg stemmed from the hydrotalcite and Al was derived from both hydrotalcite and gels. Given the analogous chemical composition of hydrotalcite as indicated in Fig. 12B, the relatively lower Mg/Al ratio in the paste around LWFA was due to the higher content of Al in gels. This aligned with the result of the Al/Ca ratio in Fig. 12 A.

Fig. 13D shows the Fe/(Si + Al) ratio of the paste around sand and LWFA. It can be seen that Fe can also be incorporated into the paste. In PC systems rich in ferrite, Fe can participate in the formation of various hydrates such as Fe-containing siliceous hydrogarnet, alumina ferric monosulfate and Fe-ettringite [73–75]. In addition, Fe(III) has been verified to be uptake by C-S-H gels, with a stronger sorption capacity than Al(III). However, due to the lower solubility of $Fe(OH)_3$ than Al $OH)_3$, the uptake of Fe by gels is quite limited.

As shown in Fig. 13D, most data points of the paste around sand show negligible Fe content, with a mean Fe/Si ratio of about 0.001, which is significantly lower than the ratio in pastes around LWFA (0.006). This difference was due to the higher Fe₂O₃ content in LWFA (9 %) compared to slag (0.6 %). As stated in [74], Fe(III) is octahedrally coordinated within the interlayers of gels with high Ca/Si ratios (1.2 and 1.5), while Fe(III) tends to form a separate secondary Ca-Si rich phase (or cluster) in the gel with a low Ca/Si ratio (0.8). Regardless of its state in gels, the presence of additional Fe in gels might enhance the charge negativity of the paste, similar to the role of Al. This increase in charge negativity may promote cation absorption, which could also explain the elevated Na/ (Si + Al) ratios observed in pastes around LWFA.

3.3.4. Pore structure

Fig. 14 A presents the porosity of AAS mortars. The porosity of "LWFA_0%", "LWFA_20%" and "LWFA_50%" in the range of 7 nm to 400 μm was 14 %, 19.2 % and 24.5 %, respectively. This indicated that the addition of LWFA coarsens the microstructure of AAS mortars significantly. The primary reason lay in the high porosity of LWFA (49.2 %), as shown in Fig. 2, which might be much higher than that of the matrix of pastes. As indicated by the pore size distribution (**Fig. 14B**), the presence of LWFA increases the pores ranging from 50 nm to 1000 nm. While the pozzolanic effect of LWFA can promote the formation of reaction products and the densification of the interface, it was insufficient to compensate for the pores introduced by LWFA within 28 d.

According to the mixture design, the volume fractions of paste, sand

and LWFA can be calculated, as shown in Fig. 14C. The total volume of fine aggregate was 55 %, comprising sand and LWFA. Considering the porosity of LWFA (49.2 %) and sand (0 %), the porosity of paste in the mortar can be determined, as shown in Fig. 14D. In contrast to the total porosity of mortars, the porosity of the paste decreased with the addition of LWFA. This again proved that the pozzolanic and internal curing effects of LWFA are effective in densifying the adjacent paste. Additionally, it was important to note that the accuracy of the calculated paste relies on the assumption that the reaction of LWFA is limited and the change of the porosity in LWFA is minimal within 28 d.

The sorptivity test is normally carried out on dried specimens to assess the open porosity and pore connectivity of materials. However, in this study, we conducted the test directly on the mortars sealed for 28 d, without drying. These mortars were subjected to the same conditions as those used for efflorescence observation. The water sorptivity behaviour of AAS mortars over 7 d is shown in Fig. 15. Water was constantly absorbed through the capillary suction of unsaturated pores, with the sorptivity rate gradually decreasing with time. During 7 d of measurement, the water absorption of the mortar with LWFA was much lower than that without LWFA, which seemingly contradicted the MIP result in Fig. 14 A. This discrepancy arised because the MIP test was conducted on dried samples, thereby neglecting the presence of water in the pore structure under real conditions. The additional water pre-absorbed by LWFA is likely to maintain higher internal humidity within the mortar, leading to reduced water sorptivity. The lower water absorption of LWFA-based mortars aligns with the observation in Fig. 4, in which the cylinder containing LWFA shows a lower efflorescence front.

3.3.5. Strength

Fig. 16 shows the flexural strength and compressive strength of AAS mortars at 7 d and 28 d. Generally, the compressive strength of specimens increased over time, whereas the flexural strength tended to decrease, which indicated that ambient conditions adversely affected the development of flexural strength. Similar results are also found by Liu et al. [76]. Since the flexural strength is more sensitive to cracks, its reduction can be attributed to cracks induced by dry shrinkage. In contrast, compressive strength is more related to porosity. Since slag progressively reacted and gels constantly formed 7 to 28 d, the compressive strength showed positive development.

As shown in Fig. 16 A, the flexural strength of LWFA_0% at 7 d is higher than that of LWFA_20% and LWFA_50%, however by 28 d, the

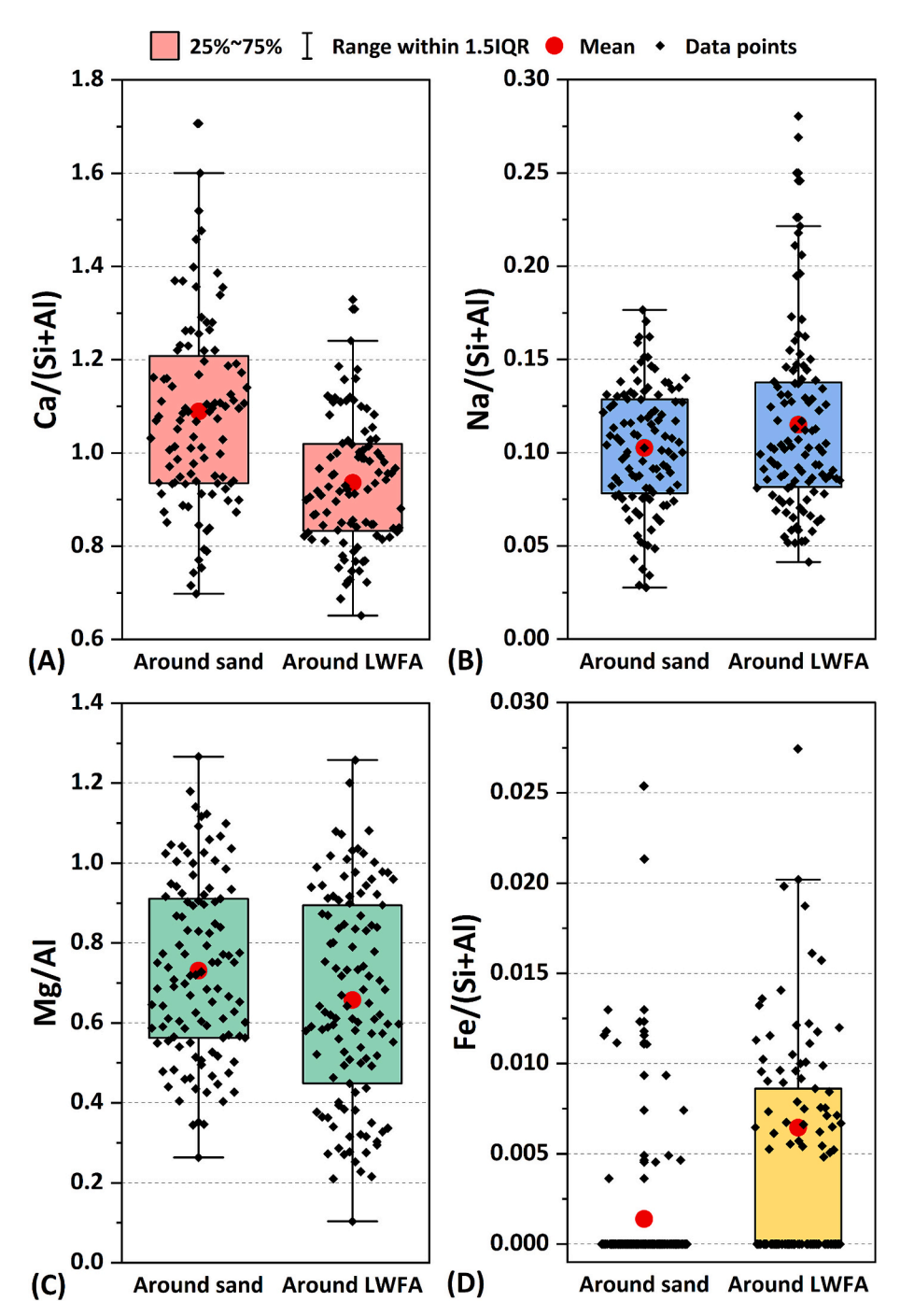


Fig. 13. Box plot of elemental ratios of the paste around sand and LWFA. In each box, 25 %–75 % indicates the data points ranging from 25th to 75th percentiles. The "IQR" indicates the interquartile range (25 %–75 %), and the whisker is located at 1.5 times of "IQR". The red circle refers to the mean value of atomic ratios. (For interpretation of the references to colour in this figure legend, the reader is referred to the web version of this article.)

flexural strength of LWFA_0% is lower than that of the mortars with LWFA. During the first 7 d, the samples were kept under sealed conditions, which largely prevented cracking, suggesting that cracks were not the main factor influencing flexural strength at this stage. The lower flexural strength of LWFA-blended mortars in the early stage can be attributed to the porous structure and lower stiffness of LWFA compared to sand. After 7 d, the samples were exposed to ambient conditions, where a reduction in environmental humidity led to water loss and dry shrinkage [77]. Due to the internal curing effect of LWFA, mortars with LWFA maintained higher internal humidity than normal mortars, which suppressed the shrinkage and cracking proneness [46]. Additionally, the pozzolanic reaction of LWFA under alkali conditions contributed to the

densification of the interface between pastes and aggregates. As a result, the flexural strength of LWFA-based mortars was higher at 28 d. Unfortunately, as shown in Fig. 16B, the compressive strength of LWFA blended mortars is constantly lower than that of the reference, with a higher substitution exhibiting a larger reduction. This was because the addition of LWFA increased the total porosity of AAS mortars, as indicated in Fig. 14 A.

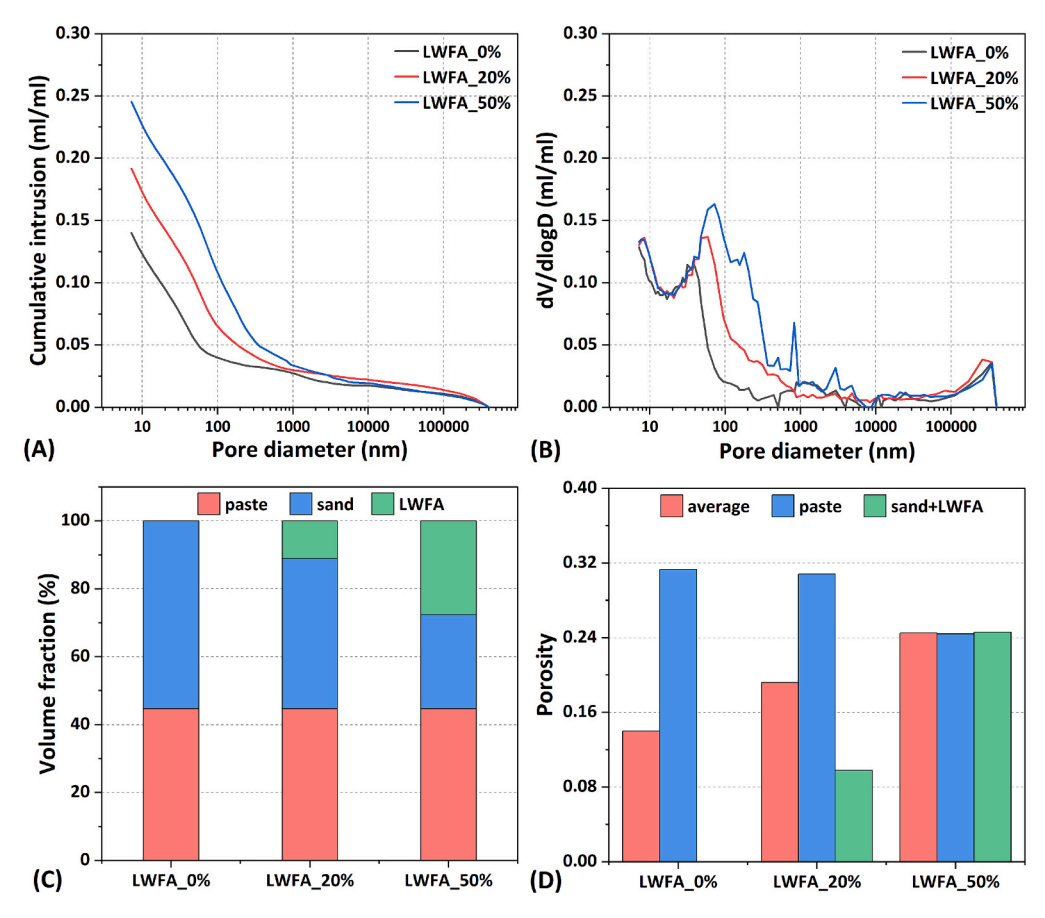


Fig. 14. (A) Pore volume and (B) pore size distribution of 28 d sealed AAS mortars; (C) volume fraction of paste and fine aggregate in AAS mortars; (D) calculated porosity of paste and aggregate in AAS mortars. The "average" in (D) indicates the mean porosity of pastes and aggregates, equivalent to the total porosity of the mortar. The porosity of sand is considered zero.

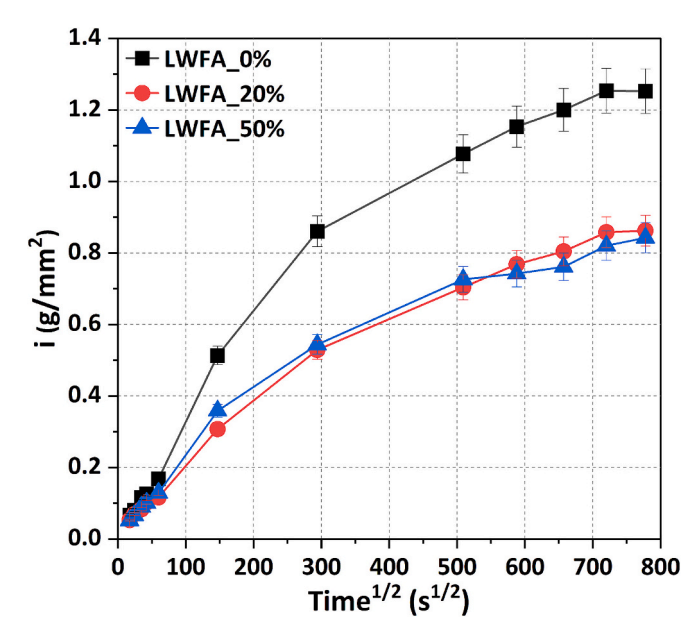


Fig. 15. Water sorptivity of 28 d sealed AAS mortars with time.

4. Discussion

4.1. Mitigating mechanisms of LWFA on the efflorescence of AAS mortars

It has been shown that the addition of LWFA can effectively mitigate

the efflorescence of AAS mortars. To better understand the underlying mechanisms, Fig. 17 shows a schematic representation of mitigation mechanisms of LWFA on the efflorescence of AAS mortars. LWFA is an aluminosilicate material containing amorphous Si and Al, which can be dissolved under alkali conditions. The experimental results show that the dissolved Si and Al species participate in the formation of gels, which results in the gel around LWFA showing a lower Ca/(Si + Al) ratio (Fig. 17 A). According to the leaching test and EDX point analyses, the gel in LWFA-based mortars has a higher uptake of Na (Fig. 17B). This is mainly because the gel with a lower Ca/(Si + Al) ratio shows higher charge negativity on the surface, allowing them to bind more Na⁺ in the pore solution [78]. Meanwhile, the constant pozzolanic reaction of LWFA reduces the pH of the pore solution. As a result, the concentration of both Na⁺ and OH⁻ in the pore solution decreases, limiting the availability of raw species necessary for the formation of efflorescence products. On the other hand, a denser ITZ is observed around LWFA than the ITZ between normal sand and the paste (Fig. 17C). This densification can be ascribed to both the pozzolanic effect and the internal curing effect of LWFA. LWFA provides gels with raw species and the preabsorbed water supports ongoing reaction. A densified pore structure inhibits ion migration and water transport, thereby mitigating the efflorescence formation.

Given the time efficiency of efflorescence experiments and the simplification of AAS systems, we mainly focused on NH mortars in this study. However, we also conducted experiments on sodium silicate-activated (NS) AAS mortars with a silicate modulus of 1. Fig. A2 shows the NS cylinders sealed for 28 d, followed by 90 d of efflorescence under ambient conditions. It can be observed that efflorescence on NS mortars developed more slowly and was less pronounced than that on

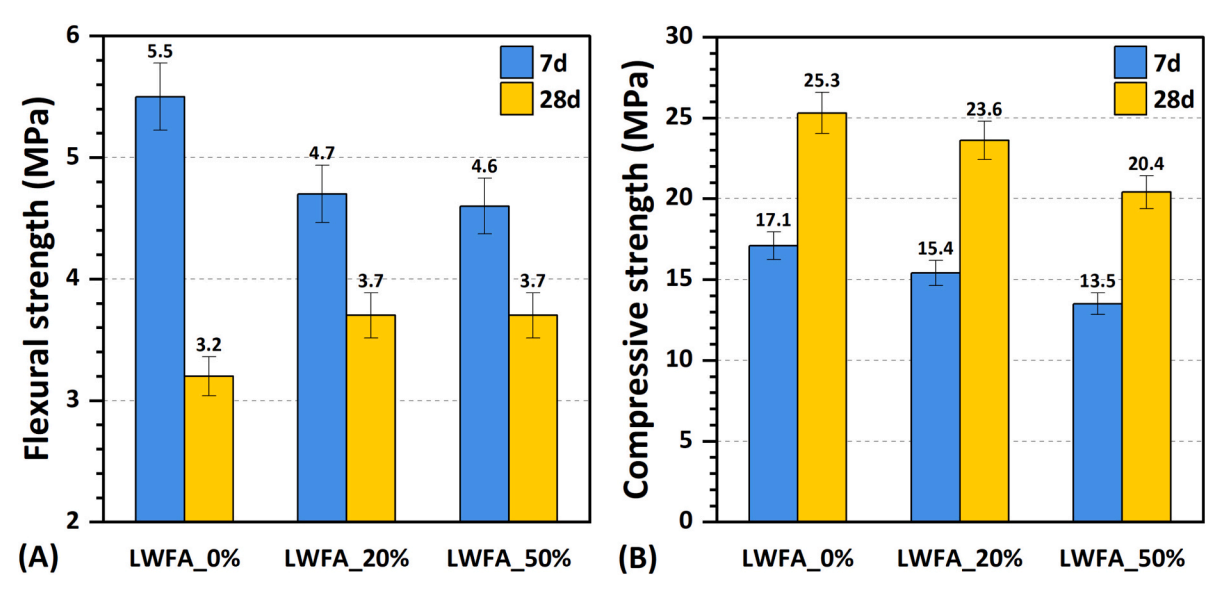


Fig. 16. Flexural and compressive strengths of AAS mortars at 7 d and 28 d. "7 d" refers to the specimen that was cured under sealed conditions for 7 d, while "28 d" denotes the specimen that was initially cured under sealed conditions for 7 d, followed by ambient curing until 28 d.

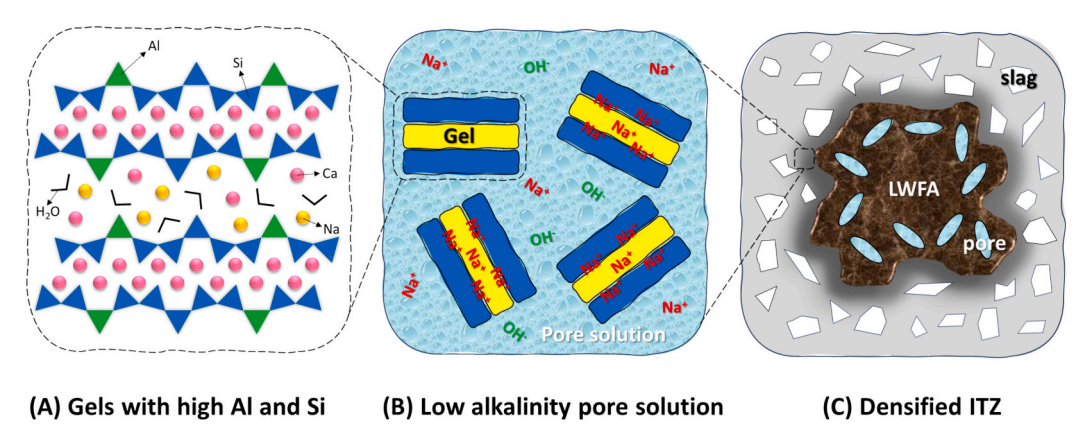


Fig. 17. Schematic representation of mitigation mechanisms of LWFA on the efflorescence of AAS mortars.

NH mortars at the same exposure age, likely due to the denser microstructure of NS mortars. However, LWFA appeared to be less effective in NS mortars during the first 28 d, as the extent of efflorescence of three NS cylinders was similar at this stage (Figs. A2 D—F). This may be attributed to the significantly higher porosity of LWFA compared to NS pastes which led to noticeable coarsening of the microstructure in NS systems when LWFA was introduced. Fortunately, after 90 d of exposure, NS mortars containing LWFA exhibited less efflorescence than those without LWFA (Figs. A2 G-I), indicating that LWFA became more effective in mitigating efflorescence in NS mortars over an extended period.

4.2. Advantages and limitations of LWFA in AAS materials

In addition to its effectiveness in mitigating efflorescence, LWFA also shows promise in reducing the cracking potential of AAS mortars, particularly in NS systems. Fig. A3 shows the surface appearance of three NS cylinders sealed for 28 d. The surface of the "LWFA_0%" cylinder was covered with microcracks, whereas the surfaces of the "LWFA_20%" and "LWFA_50%" cylinders were smooth and free of visible cracks. This was probably attributed to the release from wet LWFA during the early reaction of slag, which was conducive to impeding the shrinkage and cracking potential induced by self-desiccation [45,79]. This is meaningful for the application of AAS concrete, as it typically shows larger

shrinkage compared to traditional cementitious materials.

Although LWFA has a porous structure and lower stiffness than sand, the compressive strength of the "LWFA_20%" mortar only decreased by 6.7 % compared to the "LWFA_0%" mortar at 28 d (Fig. 16 A). Interestingly, the flexural strength of LWFA-based mortars was 15.6 % higher than that of mortar without LWFA (Fig. 16B), likely due to the internal curing effect of LWFA, which helped to prevent the formation of microcracks. In cementitious materials, elevated temperatures and chemical agents are commonly employed to enhance the pozzolanic reactivity of LWFA [69,80]. However, in AAM systems, it is plausible that the naturally high alkaline conditions can provide LWFA with a favourable environment for satisfactory reactivity without the need for additional treatments. The results of this work highlighted the excellent adaptability of LWFA in AAMs.

5. Conclusions

In this study, the efflorescence of AAS mortars with and without aluminosilicate-based LWFA under ambient conditions was investigated. The impacts of LWFA on the properties of AAS mortars were comprehensively investigated. The mitigation mechanisms of LWFA on the efflorescence of AAS mortars and some prospective were revealed. The conclusions of this study are drawn as follows.

- 1. LWFA can effectively mitigate the efflorescence of AAS mortars. Substituting sand with LWFA by 20 % or 50 % in volume reduced the efflorescence of AAS mortars by 14.6 % or 43 %, respectively. LWFA-based mortars exhibited a lower efflorescence front than that of normal mortars. Additionally, the efflorescence product (thermonatrite) in mortars with and without LWFA was the same.
- 2. Leaching of Na from fresh AAS mortar pieces decreased as the dosage of LWFA increased, while that from dried powdered AAS mortar increased with the dosage of LWFA. This indicated that the presence of LWFA reduced the Na content in the pore solution and enhanced the binding of Na within the gel structure.
- 3. The dissolution test of LWFA in the NH activator, along with the ion concentration analysis of the pore solution, demonstrated that LWFA consumed OH⁻ and Na⁺ ions in the solution and promoted the dissolution of Si and Al. These additional Si and Al species contributed to the formation of gels and densification of microstructure.
- 4. The introduction of LWFA increased the total porosity of AAS mortars at 28 d but reduced the porosity of pastes. The mortar containing LWFA showed lower water absorption due to the extra water introduced by LWFA. This resulted in a lower efflorescence front of LWFA-based mortars than normal mortars.
- 5. In spite of the porous structure of LWFA, the compressive strength of LWFA_20% mortar was only 6.7 % lower than that of the LWFA_0% mortar. The internal curing effect of LWFA improved the flexural strength of both LWFA_20% and LWFA_50% mortars by 15.6 % compared to normal mortar. This indicated the excellent adaptability of LWFA in AAS materials, suggesting its promising application potential in AAMs.

6. The synergistic effect of internal curing and the pozzolanic reaction of LWFA contributed to the densification of the ITZ by the additional formation of gels. A denser matrix reduced the transport of ions and water, thereby mitigating efflorescence. Furthermore, these extra gels showed lower Ca/(Si + Al) ratios, which enhanced the Na binding in the pore solution, reducing the amount of free Na available for efflorescence.

CRediT authorship contribution statement

Chen Liu: Writing – original draft, Methodology, Investigation, Conceptualization. **Zhenming Li:** Writing – review & editing, Investigation. **Guang Ye:** Writing – review & editing, Supervision.

Declaration of competing interest

The authors declare that they have no known competing financial interests or personal relationships that could have appeared to influence the work reported in this paper.

Acknowledgements

Chen Liu would like to acknowledge the funding supported by the China Scholarship Council (CSC) under grant No. 201906950102. Zhenming Li would like to acknowledge the Guangdong Provincial Key Laboratory of Intelligent and Resilient Structures for Civil Engineering (2023B1212010004).

Appendix A

Fig. A1 shows the appearance of aluminosilicate-based LWFA used in this study.



Fig. A1. Appearance of aluminosilicate-based LWFA.

Fig. A2 shows the efflorescence of NS-activated (sodium silicate-activated) AAS mortars under ambient conditions with time. It can be seen that the efflorescence of the three NS mortars at 28 d was comparable, while the efflorescence of two LWFA-based NS mortars was lower than that of the normal mortars at 90 d.



Fig. A2. Visual observation of efflorescence of NS-activated AAS mortars with time.

Fig. A3 shows the surface of NS mortar cylinders sealed for 28 d. The surface of the mortar without LWFA (LWFA_0%) was covered by microcracks while that of the two mortars containing LWFA (LWFA_20% and LWFA_50%) showed no visible cracks on the surface.

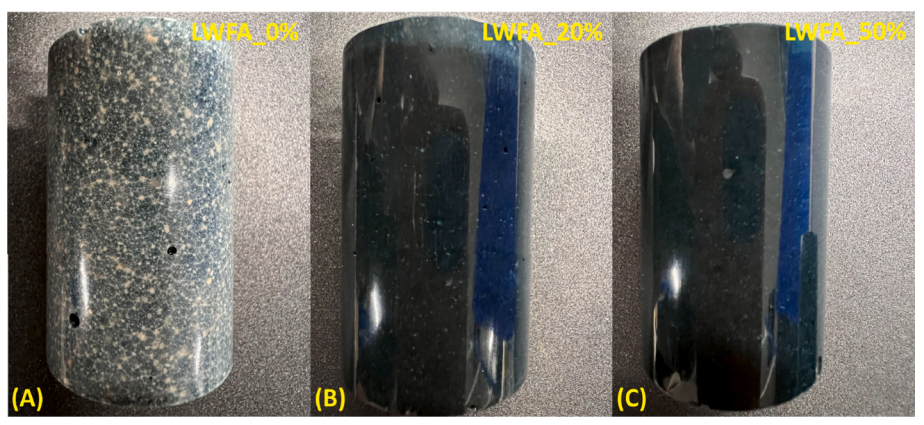


Fig. A3. Appearance of NS-activated AAS mortar cylinders after 28 d of sealed curing.

Data availability

Data will be made available on request.

References

- [1] P. Russell, Efflorescence and the Discoloration of Concrete, CRC Press, 1983.
- [2] A. Allahverdi, E. Najafi Kani, K.M.A. Hossain, M. Lachemi, Methods to control efflorescence in alkali-activated cement-based materials, Handb. Alkali-Activated Cem. Mortars Concr. (2015) 463–483, https://doi.org/10.1533/ 9781782422884.3.463.
- [3] C. Dow, F.P. Glasser, Calcium carbonate efflorescence on Portland cement and building materials, Cem. Concr. Res. 33 (2003) 147–154, https://doi.org/10.1016/ S0008-8846(02)00937-7.
- [4] H. Brocken, T.G. Nijland, White efflorescence on brick masonry and concrete masonry blocks, with special emphasis on sulfate efflorescence on concrete blocks, Constr. Build. Mater. 18 (2004) 315–323, https://doi.org/10.1016/j. conbuildmat.2004.02.004.

- [5] C. Liu, Z. Li, S. Nie, S. Skibsted, G. Ye, Structural evolution of calcium sodium aluminosilicate hydrate (C-(N-)A-S-H) gels induced by water exposure: the impact of Na leaching, Cem. Concr. Res. 178 (2024), https://doi.org/10.1016/j. cem.conres.2024.107432.
- [6] M.A. Longhi, Z. Zhang, B. Walkley, E.D. Rodríguez, A.P. Kirchheim, Strategies for control and mitigation of efflorescence in metakaolin-based geopolymers, Cem. Concr. Res. 144 (2021), https://doi.org/10.1016/j.cemconres.2021.106431.
- [7] Z. Zhang, J.L. Provis, A. Reid, H. Wang, Fly ash-based geopolymers: the relationship between composition, pore structure and efflorescence, Cem. Concr. Res. 64 (2014) 30–41, https://doi.org/10.1016/j.cemconres.2014.06.004.
- [8] Z. Zhang, J.L. Provis, X. Ma, A. Reid, H. Wang, Efflorescence and subflorescence induced microstructural and mechanical evolution in fly ash-based geopolymers, Cem. Concr. Compos. 92 (2018) 165–177, https://doi.org/10.1016/j. cemconcomp.2018.06.010.
- [9] X. Xue, Y.L. Liu, J.G. Dai, C.S. Poon, W.D. Zhang, P. Zhang, Inhibiting efflorescence formation on fly ash–based geopolymer via silane surface modification, Cem. Concr. Compos. 94 (2018) 43–52, https://doi.org/10.1016/j. cemconcomp.2018.08.013.
- [10] M.A. Longhi, E.D. Rodríguez, B. Walkley, Z. Zhang, A.P. Kirchheim, Metakaolinbased geopolymers: relation between formulation, physicochemical properties and

- efflorescence formation, Compos. Part B Eng. 182 (2020), https://doi.org/10.1016/j.compositesb.2019.107671.
- [11] Z. Zhang, H. Wang, J.L. Provis, A. Reid, Efflorescence: A Critical Challenge for Geopolymer Applications? Concr. Inst. Aust. Bienn. Natl, Conf., 2013.
- [12] L. Feng, S. Yi, S. Zhao, Q. Zhong, F. Ren, C. Liu, Y. Zhang, W. Wang, N. Xie, Z. Li, N. Cui, Recycling of Aluminosilicate-based solid wastes through alkali-activation: preparation, characterization, and challenges, Buildings 14 (2024), https://doi.org/10.3390/buildings14010226.
- [13] A. Allahverdi, E. Najafi Kani, B. Shaverdi, Carbonation versus efflorescence in alkali-activated blast-furnace slag in relation with chemical composition of activator, Int. J. Civ. Eng. 15 (2017) 565–573, https://doi.org/10.1007/s40999-017-0225-4.
- [14] L. Srinivasamurthy, V.S. Chevali, Z. Zhang, A. Longhi, T.W. Loh, H. Wang, Mechanical property and microstructure development in alkali activated fly ash slag blends due to efflorescence, Constr. Build. Mater. 332 (2022), https://doi.org/ 10.1016/j.conbuildmat.2022.127273.
- [15] H. Maghsoodloorad, A. Allahverdi, Efflorescence formation and control in alkaliactivated phosphorus slag cement, Int. J. Civ. Eng. 14 (2016) 425–438, https://doi. org/10.1007/s40999-016-0027-0.
- [16] F. Škvára, L. Kopecký, L. Myšková, V.Í.T. Šmilauer, L. Alberovská, L. Vinšová, Aluminosilicate polymers - influence of elevated temperatures, efflorescence, Ceramics-Silikáty 53 (2009) 276–282.
- [17] X. Yao, T. Yang, Z.Z. Zhang, Y. Wang, X. Liu, W.D. Zhang, Z. Li, Y. Zhang, Y. Li, Y. Ren, K. Sun, X. Peng, S. Wang, L. Zeng, P. Ran, G. Ji, M.A. Longhi, E. D. Rodríguez, B. Walkley, Z.Z. Zhang, A.P. Kirchheim, S.P. Kang, S.J. Kwon, X. Xue, Y.L. Liu, J.G. Dai, C.S. Poon, W.D. Zhang, P. Zhang, Z.Z. Zhang, J.L. Provis, X. Ma, A. Reid, H. Wang, J.L. Provis, A. Reid, X. Yao, T. Yang, Z.Z. Zhang, J.L. Provis, A. Reid, H. Wang, R.R. Lloyd, J.L. Provis, J.S.J. Van Deventer, Compressive strength development and shrinkage of alkali-activated fly ash–slag blends associated with efflorescence, Mater. Struct. 49 (2016) 165–177, https://doi.org/10.1016/j.cemconcomp.2018.06.010.
- [18] X. Yao, T. Yang, Z. Zhang, Fly ash-based geopolymers: effect of slag addition on efflorescence, J. Wuhan Univ. Technol. Mater. Sci. Ed. 31 (2016) 689–694, https://doi.org/10.1007/s11595-016-1430-8.
- [19] I. Ismail, S.A. Bernal, J.L. Provis, R. San Nicolas, S. Hamdan, J.S.J. Van Deventer, Modification of phase evolution in alkali-activated blast furnace slag by the incorporation of fly ash, Cem. Concr. Compos. 45 (2014) 125–135, https://doi. org/10.1016/j.cemconcomp.2013.09.006.
- [20] L. Srinivasamurthy, V.S. Chevali, Z. Zhang, H. Wang, Phase changes under efflorescence in alkali activated materials with mixed activators, Constr. Build. Mater. 283 (2021) 122678, https://doi.org/10.1016/j.conbuildmat.2021.122678.
- [21] X. Liu, E. Liu, Y. Fu, Reduction in drying shrinkage and efflorescence of recycled brick and concrete fine powder-slag-based Geopolymer, Appl. Sci. 13 (2023), https://doi.org/10.3390/app13052997.
- [22] X. Lu, Y. Tian, I.M. Jiskani, W. Zhou, B. Zhao, X. Ding, Z. Ao, Innovate geopolymer synthesis for green mine road construction: analysis of efflorescence behavior and strength analysis, Constr. Build. Mater. 401 (2023) 132963, https://doi.org/ 10.1016/j.conbuildmat.2023.132963.
- [23] K. Hyeok-Jung, S.P. Kang, G.C. Choe, Effect of red mud content on strength and efflorescence in pavement using alkali-activated slag cement, Int. J. Concr. Struct. Mater. 12 (2018), https://doi.org/10.1186/s40069-018-0258-3.
- [24] E. Najafi Kani, A. Allahverdi, J.L. Provis, Efflorescence control in geopolymer binders based on natural pozzolan, Cem. Concr. Compos. 34 (2012) 25–33, https:// doi.org/10.1016/j.cemconcomp.2011.07.007.
- [25] R. Zhang, Y. Zhang, T. Liu, Q. Wan, D. Zheng, Effect of high alumina-based solid waste on efflorescence behavior of alkali-activated steel slag, Constr. Build. Mater. 349 (2022) 128804, https://doi.org/10.1016/j.conbuildmat.2022.128804.
- 349 (2022) 128804, https://doi.org/10.1016/j.conbuildmat.2022.128804.

 [26] Tao Liu, Yuxuan Chen, Bo Yuan, Weitan Zhuang, H.J.H. Brouwers, Qingliang Yu, sodium aluminate activated waste glass: reduced efflorescence behavior by C(N)—a—S—H transformation, Cem. Concr. Res. 181 (2024) 107527, https://doi.org/10.1016/j.cemconres.2024.107527.
- [27] J.B. Wang, F.S. Li, Z.H. Zhou, P. Du, D. Xu, N. Xie, X. Cheng, Y. Liu, Effect of zeolite on waste based alkali-activated inorganic binder efflorescence, Constr. Build. Mater. 158 (2018) 683–690, https://doi.org/10.1016/j.conbuildmat.2017.10.065.
 [28] X. Huang, S. Hu, F. Wang, Y. Liu, Y. Mu, Properties of alkali-activated slag with
- [28] X. Huang, S. Hu, F. Wang, Y. Liu, Y. Mu, Properties of alkali-activated slag with addition of cation exchange material, Constr. Build. Mater. 146 (2017) 321–328, https://doi.org/10.1016/j.conbuildmat.2017.03.127.
- [29] J. Wang, T. Zhou, D. Xu, Z. Zhou, P. Du, N. Xie, X. Cheng, Y. Liu, Effect of nanosilica on the efflorescence of waste based alkali-activated inorganic binder, Constr. Build. Mater. 167 (2018) 381–390, https://doi.org/10.1016/j. conbuildmat.2018.02.006.
- [30] F. Matalkah, A. Ababneh, R. Aqel, Efflorescence control in calcined kaolin-based Geopolymer using silica fume and OPC, J. Mater. Civ. Eng. 33 (2021) 2–9, https://doi.org/10.1061/(asce)mt.1943-5533.0003764.
- [31] A. Saludung, T. Azeyanagi, Y. Ogawa, K. Kawai, Effect of silica fume on efflorescence formation and alkali leaching of alkali-activated slag, J. Clean. Prod. 315 (2021) 128210, https://doi.org/10.1016/j.jclepro.2021.128210.
- [32] B. Wu, X. Ma, H. Deng, Y. Li, Y. Xiang, Y. Zhu, An efficient approach for mitigation of efflorescence in fly ash-based geopolymer mortars under high-low humidity cycles, Constr. Build. Mater. 317 (2022), https://doi.org/10.1016/j. conbuildmat.2021.126159.
- [33] K. Pasupathy, S. Ramakrishnan, J. Sanjayan, Effect of hydrophobic surface-modified fine aggregates on efflorescence control in geopolymer, Cem. Concr. Compos. 126 (2022) 104337, https://doi.org/10.1016/j.cemconcomp.2021.104337.

- [34] D. Tang, C. Yang, X. Li, X. Zhu, K. Yang, L. Yu, Mitigation of efflorescence of alkaliactivated slag mortars by incorporating calcium hydroxide, Constr. Build. Mater. 298 (2021) 123873, https://doi.org/10.1016/j.conbuildmat.2021.123873.
- [35] Y. Zhao, B. Chen, H. Duan, Effect of rice husk ash on properties of slag based geopolymer pastes, J. Build. Eng. 76 (2023) 107035, https://doi.org/10.1016/j. jobe.2023.107035.
- [36] S. Hasdemir, A. Tuğrul, M. Yılmaz, The effect of natural sand composition on concrete strength, Constr. Build. Mater. 112 (2016) 940–948.
- [37] Y. Zhao, X. Hu, C. Shi, Z. Zhang, D. Zhu, A review on seawater sea-sand concrete: mixture proportion, hydration, microstructure and properties, Constr. Build. Mater. 295 (2021) 123602, https://doi.org/10.1016/j.conbuildmat.2021.123602.
- [38] M. Selva Ganesh, P. Jagadeesh, Assessment of usage of manufactured sand and recycled aggregate as sustainable concrete: a review, Mater. Today Proc. 64 (2022) 1029–1034, https://doi.org/10.1016/j.matpr.2022.05.094.
- [39] L. Kong, L. Hou, Y. Du, Chemical reactivity of lightweight aggregate in cement paste, Constr. Build. Mater. 64 (2014) 22–27, https://doi.org/10.1016/j. conbuildmat.2014.04.024.
- [40] S. Nie, S. Hu, F. Wang, C. Hu, X. Li, Y. Zhu, Pozzolanic reaction of lightweight fine aggregate and its influence on the hydration of cement, Constr. Build. Mater. 153 (2017) 165–173
- [41] A. Bentur, S.I. Igarashi, K. Kovler, Prevention of autogenous shrinkage in highstrength concrete by internal curing using wet lightweight aggregates, Cem. Concr. Res. 31 (2001) 1587–1591, https://doi.org/10.1016/S0008-8846(01)00608-1.
- [42] D. Cusson, T. Hoogeveen, Internal curing of high-performance concrete with presoaked fine lightweight aggregate for prevention of autogenous shrinkage cracking, Cem. Concr. Res. 38 (2008) 757–765, https://doi.org/10.1016/j.cem.concres.2008.02.001.
- [43] P. Risdanareni, K. Schollbach, J. Wang, N. De Belie, The effect of NaOH concentration on the mechanical and physical properties of alkali activated fly ash-based artificial lightweight aggregate, Constr. Build. Mater. 259 (2020) 119832, https://doi.org/10.1016/j.conbuildmat.2020.119832.
- [44] H.Ö. Öz, H.E. Yücel, M. Güneş, T.Ş. Köker, Fly-ash-based geopolymer composites incorporating cold-bonded lightweight fly ash aggregates, Constr. Build. Mater. 272 (2021), https://doi.org/10.1016/j.conbuildmat.2020.121963.
- [45] M.S. Tale Masoule, N. Bahrami, M. Karimzadeh, B. Mohasanati, P. Shoaei, F. Ameri, T. Ozbakkaloglu, Lightweight geopolymer concrete: a critical review on the feasibility, mixture design, durability properties, and microstructure, Ceram. Int. 48 (2022) 10347–10371, https://doi.org/10.1016/j.ceramint.2022.01.298.
- [46] X. Zheng, H. Liu, S. You, S. Easa, K. Cheng, Z. Chen, T. Ji, Cracking resistance and sustainability assessment of alkali-activated slag concrete incorporating lightweight aggregate, Cem. Concr. Compos. 131 (2022) 104556, https://doi.org/ 10.1016/j.cemconcomp.2022.104556.
- [47] P. Chen, Z. Wang, S. Cao, X. Rong, Z. Shi, H. Wang, Study on axial compressive stress-strain relationship of alkali-activated slag lightweight aggregate concrete, Constr. Build. Mater. 364 (2023) 129991, https://doi.org/10.1016/j. combuildmat.2022.129991.
- [48] S. Yang, X. Guan, J. Lu, H. Cui, C. Sun, Micromechanical and chemical characteristics of interfacial transition zone in alkali-activated slag concrete containing lightweight iron-rich aggregates, Compos. Part B 283 (2024) 111671, https://doi.org/10.1016/j.compositesb.2024.111671.
- [49] P. Chen, Z. Shi, S. Cao, P. Liu, X. Rong, L. Wang, Mechanical properties of alkaliactivated slag lightweight aggregate concrete, J. Clean. Prod. 359 (2022) 132136, https://doi.org/10.1016/j.jclepro.2022.132136.
- [50] H.M. Albegmpril, Z.K.A. Al-Qazzaz, S.K. Rejeb, Strength performance of alkali activated structural lightweight geopolymer concrete exposed to acid, Ceram. Int. 48 (2022) 6867–6873, https://doi.org/10.1016/j.ceramint.2021.11.240.
- [51] C. Liu, L. Yang, Z. Li, S. Nie, C. Hu, F. Wang, Improve the long-term property of heat-cured mortars blended with fly ash by internal curing, J. Build. Eng. 54 (2022) 104624, https://doi.org/10.1016/j.jobe.2022.104624.
- [52] C. D.V.S.K, N. Satish Kumar Ch, A review on concrete's rheological properties, World J. Eng. 21 (2024) 53–70. doi: https://doi.org/10.1108/WJF-02-2022-0069
- World J. Eng. 21 (2024) 53–70. doi: https://doi.org/10.1108/WJE-02-2022-0069.
 [53] M. El Boukhari, O. Merroun, C. Maalouf, F. Bogard, B. Kissi, Comprehensive experimental study on mechanical properties of a structural concrete lightened by olive pomace aggregates mixed with olive mill wastewater, World J. Eng. 21 (2024) 862–881, https://doi.org/10.1108/WJE-12-2022-0514.
- [54] C. Liu, Z. Li, G. Ye, Mechanisms of efflorescence of alkali-activated slag, Cem. Concr. Compos. 155 (2025) 105811, https://doi.org/10.1016/j. cemconcomp.2024.105811.
- [55] C. Liu, X. Liang, Y. Chen, Z. Li, G. Ye, Degradation of alkali-activated slag subject to water immersion, Cem. Concr. Compos. 142 (2022), https://doi.org/10.1016/j. cemconcomp.2023.105157.
- [56] ASTM C1585-13, Standard test method for measurement of rate of absorption of water by hydraulic cement concretes, ASTM Int. 41 (2013) 1–6.
- [57] E.K.D. Benito, A.M.M. Aragoncillo, F.A.A. Pascua, J.M. Juanites, M.A. Eneria, R. G. Zafra, M.S. Madlangbayan, Durability performance of concrete containing recycled coarse aggregates derived from laboratory-tested specimens, World J. Eng. 21 (2024) 604–614, https://doi.org/10.1108/WJE-02-2023-0033.
- [58] B.S. En, Methods of testing cement—part 1: determination of strength, Eur. Comm. Stand. Brussels, Belgium. 169 (2005) 36.
- [59] R. Jia, Q. Wang, T. Luo, Deterioration and mitigation of efflorescence of alkaliactivated phosphorus slag, Constr. Build. Mater. 407 (2023) 133500, https://doi. org/10.1016/j.conbuildmat.2023.133500.
- [60] C. Thomas, V. Loodts, L. Rongy, A. De Wit, Convective dissolution of CO2 in reactive alkaline solutions: active role of spectator ions, Int. J. Greenh. Gas Control. 53 (2016) 230–242, https://doi.org/10.1016/j.ijggc.2016.07.034.

- [61] C. Liu, Y. Zhang, M. Liang, Z. Li, G. Ye, Underwater carbonation of alkali-activated slag pastes, Constr. Build. Mater. 445 (2024) 137967, https://doi.org/10.1016/j. conbuildmat.2024.137967.
- [62] R. Snellings, J. Chwast, Ö. Cizer, N. De Belie, Y. Dhandapani, P. Durdzinski, J. Elsen, J. Haufe, D. Hooton, C. Patapy, M. Santhanam, K. Scrivener, D. Snoeck, L. Steger, S. Tongbo, A. Vollpracht, F. Winnefeld, B. Lothenbach, RILEM TC-238 SCM recommendation on hydration stoppage by solvent exchange for the study of hydrate assemblages, Mater. Struct. Constr. 51 (2018), https://doi.org/10.1617/ s11527-018-1298-5.
- [63] R.J. Myers, E. L'Hôpital, J.L. Provis, B. Lothenbach, Composition-solubilitystructure relationships in calcium (alkali) aluminosilicate hydrate (C-(N,K-)A-S-H), Dalton Trans. 44 (2015) 13530–13544. doi: https://doi.org/10.1039/c5dt01124h.
- [64] R.J. Myers, S.A. Bernal, J.D. Gehman, J.S.J. Van Deventer, J.L. Provis, The role of al in cross-linking of alkali-activated slag cements, J. Am. Ceram. Soc. 98 (2015) 996–1004, https://doi.org/10.1111/jace.13360.
- [65] N. Meftah, M.S. Mahboub, Spectroscopic characterizations of sand dunes minerals of El-Oued (northeast Algerian Sahara) by FTIR, XRF and XRD analyses, Silicon 12 (2020) 147–153, https://doi.org/10.1007/s12633-019-00109-5.
- [66] F. Spectroscopy, Structure of calcium silicate hydrate (C-S-H): near-, mid-, and far-infrared, Spectroscopy 48 (1999) 742–748.
- [67] Y. Chen, Y. Mao, L. Yang, W. Wei, Q. Meng, J. Cai, A comprehensive review of factors affecting dynamic capillary effect in two-phase flow, Transp. Porous Media 144 (2022) 33–54, https://doi.org/10.1007/s11242-021-01723-x.
- [68] Y. Gao, G. De Schutter, G. Ye, Z. Tan, K. Wu, The ITZ microstructure, thickness and porosity in blended cementitious composite: effects of curing age, water to binder ratio and aggregate content, Compos. Part B Eng. 60 (2014) 1–13, https://doi.org/ 10.1016/j.compositesb.2013.12.021.
- [69] C. Liu, L. Yang, F. Wang, S. Hu, Enhance the durability of heat-cured mortars by internal curing and pozzolanic activity of lightweight fine aggregates, Constr. Build. Mater. 270 (2021) 121439, https://doi.org/10.1016/j. conbuildmat.2020.121439.

- [70] Minhong zhang; Odd E. Qjørv, Pozzolanic reactivity of lightweight aggregates, Cem. Concr. Res. 20 (1990) 884–890.
- [71] A. Elsharief, M.D. Cohen, J. Olek, Influence of lightweight aggregate on the microstructure and durability of mortar, Cem. Concr. Res. 35 (2005) 1368–1376.
- [72] H.F.W. Taylor, Cement Chemistry, Thomas Telford London, 1997.
- [73] B.Z. Dilnesa, B. Lothenbach, G. Renaudin, A. Wichser, D. Kulik, Synthesis and characterization of hydrogarnet Ca3(Al xFe1 - X)2(SiO4)y(OH) 4(3 - y), Cem. Concr. Res. 59 (2014) 96–111, https://doi.org/10.1016/j.cemconres.2014.02.001.
- [74] A. Mancini, E. Wieland, G. Geng, R. Dähn, J. Skibsted, B. Wehrli, B. Lothenbach, Fe (III) uptake by calcium silicate hydrates, Appl. Geochem. 113 (2020), https://doi. org/10.1016/j.apgeochem.2019.104460.
- [75] B.Z. Dilnesa, E. Wieland, B. Lothenbach, R. Dähn, K.L. Scrivener, Fe-containing phases in hydrated cements, Cem. Concr. Res. 58 (2014) 45–55, https://doi.org/ 10.1016/j.cemconres.2013.12.012.
- [76] C. Liu, W. Haoming, L. Zhenming, S. Hu, Y. Guang, Effect of curing condition on mechanical properties and durability of alkali-activated slag mortar, Constr. Build. Mater. 439 (2024) 137376, https://doi.org/10.1016/j.conbuildmat.2024.137376.
- [77] F. Collins, J.G. Sanjayan, Microcracking and strength development of alkali activated slag concrete, Cem. Concr. Compos. 23 (2001) 345–352, https://doi.org/ 10.1016/S0958-9465(01)00003-8.
- [78] C. Liu, Y. Tao, S. Nie, Y. Chen, Z. Li, C. Sun, Dissolution of cations in C- (N,K-) A-S-H gels at the nanoscale, Compos. Part B 297 (2025) 112337. doi: https://doi.org/10.1016/j.compositesb.2025.112337.
- [79] C. Liu, J. Xie, Z. Li, G. Ye, An experimental and numerical study on the cracking of alkali-activated slag pastes induced by water immersion, Cem. Concr. Res. 193 (2025) 107877, https://doi.org/10.1016/j.cemconres.2025.107877.
- [80] C. Liu, Y. Liu, Z. Liu, C. Hu, X. Huang, L. Yang, F. Wang, Heat-cured concrete: improving the early strength and pore structure by activating aluminosilicate internal curing agent with triisopropanolamine, J. Am. Ceram. Soc. 102 (2019) 6227–6238, https://doi.org/10.1111/jace.16458.